AD_____

AWARD NUMBER: W81XWH-08-1-0117

TITLE: Novel Optical Methods for Identification, Imaging, and Preservation of the Cavernous Nerves Responsible for Penile Erections during Prostate Cancer Surgery

PRINCIPAL INVESTIGATOR: Nathaniel M. Fried, Ph.D.

CONTRACTING ORGANIZATION: University of North Carolina at Charlotte
Charlotte, NC 28223

REPORT DATE: March 2010

TYPE OF REPORT: Annual

PREPARED FOR: U.S. Army Medical Research and Materiel Command
Fort Detrick, Maryland 21702-5012

REPORT DOCUMENTATION PAGE

Form Approved
OMB No. 0704-0188

1. REPORT DATE	2. REPORT TYPE	3. DATES COVERED
1 March 2010	Annual	1 Mar 2009 – 28 Feb 2010

4. TITLE AND SUBTITLE

Novel Optical Methods for Identification, Imaging, and Preservation of the Cavernous Nerves Responsible for Penile Erections during Prostate Cancer Surgery

5a. CONTRACT NUMBER

5b. GRANT NUMBER
W81XWH-08-1-0117

5c. PROGRAM ELEMENT NUMBER

6. AUTHOR(S)

Nathaniel M. Fried, Ph.D.

E-Mail: nmfried@uncc.edu

5d. PROJECT NUMBER

5e. TASK NUMBER

5f. WORK UNIT NUMBER

7. PERFORMING ORGANIZATION NAME(S) AND ADDRESS(ES)

University of North Carolina at Charlotte
Charlotte, NC 28223

8. PERFORMING ORGANIZATION REPORT NUMBER

9. SPONSORING / MONITORING AGENCY NAME(S) AND ADDRESS(ES)
U.S. Army Medical Research and Materiel Command
Fort Detrick, Maryland 21702-5012

10. SPONSOR/MONITOR'S ACRONYM(S)

11. SPONSOR/MONITOR'S REPORT NUMBER(S)

12. DISTRIBUTION / AVAILABILITY STATEMENT
Approved for Public Release; Distribution Unlimited

13. SUPPLEMENTARY NOTES

14. ABSTRACT

There is wide variability in sexual potency rates (9-86%) after prostate cancer surgery due to a limited understanding of the location of the cavernous nerves, which are responsible for erectile function. Advances in identification and preservation of these nerves would result in improved postoperative potency and patient quality of life. We hypothesize that application of 3 optical technologies for identification, imaging, and preservation of the nerves during prostate surgery will result in improved sexual function: (1) Laser nerve stimulation for identification, (2) optical coherence tomography (OCT) for nerve imaging, and (3) precise laser prostate dissection for nerve preservation. In Year 2, we continued development and testing of the laser nerve stimulation probe, measured the near-infrared optical properties of the prostate for optimization of OCT imaging, and combined 3 image processing algorithms for improving image quality of OCT prostate images. This work resulted in the publication of 2 manuscripts, 5 conference proceedings, and 1 abstract.

15. SUBJECT TERMS
Laser Nerve Stimulation; Optical Coherence Tomography; Cavernous Nerves

16. SECURITY CLASSIFICATION OF:			17. LIMITATION OF ABSTRACT	18. NUMBER OF PAGES	19a. NAME OF RESPONSIBLE PERSON
a. REPORT	b. ABSTRACT	c. THIS PAGE			19b. TELEPHONE NUMBER *(include area code)*
U	U	U	UU	49	USAMRMC

Standard Form 298 (Rev. 8-98)
Prescribed by ANSI Std. Z39.18

TABLE OF CONTENTS

INTRODUCTION

One of the greatest challenges of prostate cancer surgery is preservation of sexual function after surgery. There has been a wide variability in reported post-operative potency rates, ranging from 9 - 86%. This variability may be due, in part, to our limited understanding of the location, extent, and course of the cavernous nerves, which are responsible for erectile function. Because of the close proximity of the nerves to the surface of the prostate, they are at risk of damage during surgical dissection and removal of a cancerous prostate gland. In addition, their microscopic nature makes it difficult to predict the true course and location of these nerves from one individual patient to another. Improvements in identification, imaging, and visualization of these nerves will likely improve the consistency of nerve preservation and postoperative potency and thus lead to an improved quality of life for patients.

We hypothesize that the application of novel optical technologies for identification, imaging, and preservation of the cavernous nerves during prostate cancer surgery will result in improved sexual function. We intend to test three complementary optical technologies: Non-contact laser stimulation for identification of the cavernous nerves, high-resolution imaging of the cavernous nerves using optical coherence tomography (OCT), and rapid, precise, and hemostatic dissection of the prostate from the cavernous nerves using a KTP laser.

Year 1 was devoted to optimization of the laser nerve stimulation parameters and direct comparison with conventional electrical nerve stimulation. We completed these tasks ahead of schedule, and therefore started work on some of the Year 2 aims as well, such as assembly of a laparoscopic laser nerve stimulation probe, and improving the image quality of optical coherence tomography for differentiating the cavernous nerves from the prostate gland. The Year 1 work resulted in the publication of 2 manuscripts, 5 conference proceedings, and 3 abstracts, as stated in the Year 1 Report.

In Year 2, we continued the development and testing of the laparoscopic laser nerve stimulation probe, incorporating laser beam collimation and laser beam shaping methods into the device. This resulted in faster and stronger stimulation at shorter durations than previously reported using the conventional probe design. We also measured the optical properties of the prostate gland at several near-infrared laser wavelengths for potential use with optical coherence tomography (OCT) systems. Our study found improved optical penetration depth at 1064 nm in comparison with the conventional 1310 nm wavelength currently used in OCT. Finally, we combined the application of three complementary image processing algorithms (denoising, segmentation, and edge detection) to OCT images of the rat prostate and cavernous nerves to improve the signal to noise ratio, contrast to noise ratio, and imaging depth. In summary, during Year 2 of the grant, we published 2 manuscripts, 5 conference proceedings, and 1 abstract. Our research results were also presented at several national and international conferences, including the International Symposium for Biomedical Optics (SPIE), the Engineering and Urology Society (EUS) annual meeting, and the Optical Society of America (OSA) Biomedical Symposium.

BODY

STATEMENT OF WORK (Year 2)

TASK #1 (cont). Laser stimulation of cavernous nerves (Months 1-18).

C. Develop rapid scanning laser nerve stimulation system for prostate surgery (Months 13-18).

***Objectives*:** Develop laparoscopic laser nerve stimulation probe capable of rapid scanning of tissue, identification of cavernous nerves during prostate cancer surgery.

***Criteria for Success*:** Develop laparoscopic laser stimulation probe with rapid scanning capability, and with 4-mm-OD for insertion through 5-mm-ID laparoscopic port during prostate surgery.

***Status*:** Started during Year 1 (see Year 1 Report) and Completed during Year 2.

***Results*:**

Noncontact laser stimulation of the cavernous nerves was previously demonstrated in a rat model, *in vivo*, as a potential alternative to electrical nerve stimulation for identification of the CN's during prostate surgery. However, the therapeutic window for ONS is narrow, so optimal design of the fiber optic delivery system is critical for safe, reproducible stimulation. This study describes modeling, assembly, and testing of an ONS probe for delivering a small, collimated, flat-top laser beam for uniform cavernous nerve stimulation. A direct comparison of the magnitude and response time of the intracavernosal pressure (ICP) for both Gaussian and flat-top spatial beam profiles (Figure 1) was performed. Thulium fiber laser radiation (λ=1870 nm) was delivered through a 200-μm fiber, with distal fiber tip chemically etched to convert a Gaussian to flat-top beam profile. The laser beam was collimated to a 1-mm-diameter spot using an aspheric lens. Computer simulations of light propagation were also used to optimize the probe design.

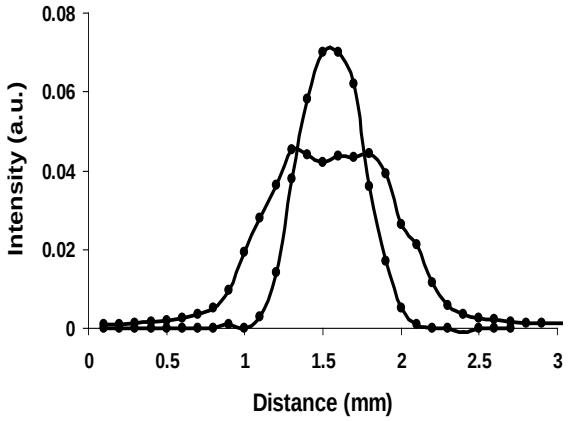

Figure 1. Comparison of Gaussian and Flat-top beam profiles at distal fiber tip of laparoscopic probe. The flat-top beam profile provides more uniform irradiation of the nerve surface, providing safer and more consistent nerve stimulation.

The 10-Fr (3.4-mm-OD) laparoscopic probe provided a constant radiant exposure at the nerve surface. The probe was tested in four rats, *in vivo*. Laser nerve stimulation of the cavernous nerves was performed with a 1-mm-diameter spot, 5-ms pulse duration, and pulse rate of 20 Hz for a duration of 15-30 s. The flat-top laser beam profile consistently produced a faster and higher ICP response at a lower radiant exposure than the Gaussian beam profile due, in part, to easier alignment of the more uniform flat-top laser beam profile with nerve (Figure 2).

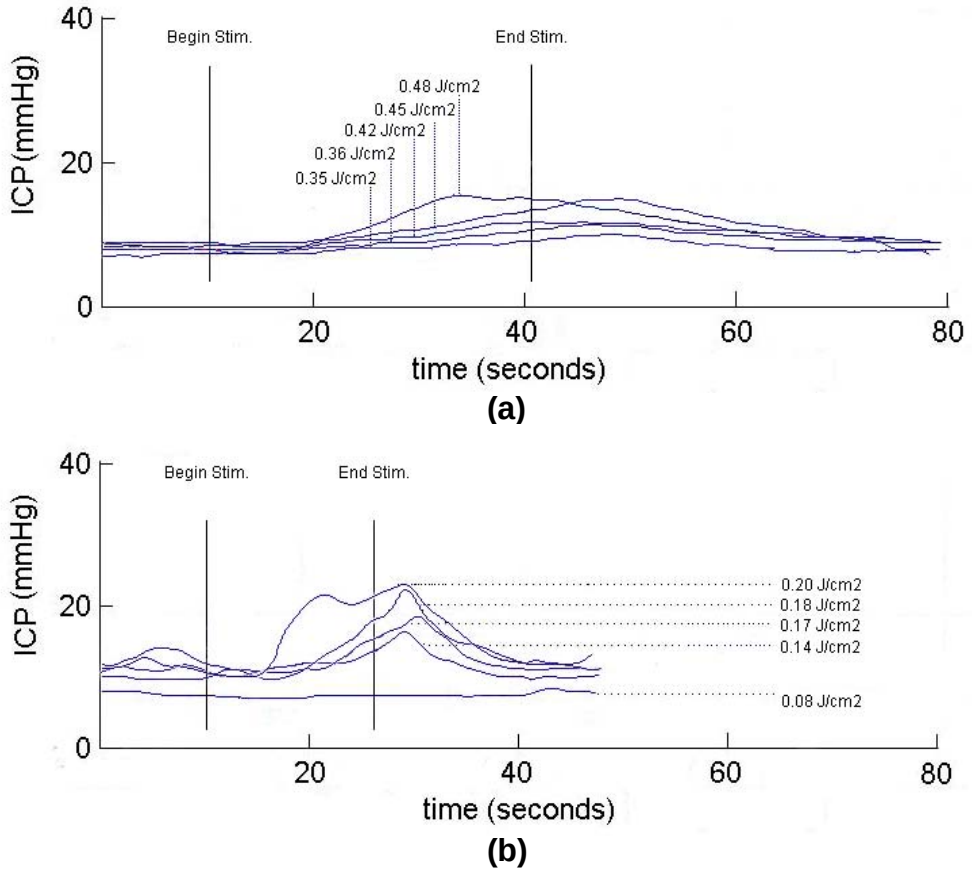

Figure 2. Comparison of (a) Gaussian and (b) flat-top spatial beam profiles for optical stimulation of the rat cavernous nerves as a function of radiant exposure. The magnitude of the ICP increases and the response time decreases as the radiant exposure is increased for both beam profiles. However, by comparison, the ICP response is significantly higher and faster for the flat-top beam profile at lower radiant exposures than for the Gaussian beam profile.

In summary, a 3.4-mm-OD laparoscopic probe capable of delivering a collimated, 1-mm-diameter, flat-top laser beam was designed and successfully tested for optical nerve stimulation. ***This probe produced a faster and higher ICP response in rat CN at a lower radiant exposure than for a standard probe with Gaussian beam profile.***

TASK #2. Image cavernous nerves using Optical Coherence Tomography (OCT).

A. Improve OCT image depth and resolution (Months 13-18).

***Objective*:** Improve OCT image depth and resolution in prostate tissue;

***Criteria for Success*:** Improve OCT image depth from 1 to 2 mm, image resolution from 11 to 7 μm.

***Status*:** Completed.

***Results*:**

The optimal wavelength for optical coherence tomography of the prostate has yet to be determined. The objective of this study was to determine the optimal near-infrared wavelength for OCT imaging of the prostate. An oblique-incidence single point measurement technique using a normal-detector scanning system was implemented to determine the absorption (μ_a) and reduced scattering coefficients (μ'_s) of fresh canine prostate tissue, *ex vivo*, from the diffuse reflectance profile

of near-IR light as a function of source-detector distance. The effective attenuation coefficient (μ_{eff}) and optical penetration depth (OPD) were then calculated for near-IR wavelengths of 1064, 1307, and 1555 nm (Table 1). A total of ten canine samples were used for this study. At wavelengths of 1064, 1307, and 1555 nm, the mean absorption coefficients measured 0.08 $\pm$ 0.03, 0.12 $\pm$ 0.04, and 0.23 $\pm$ 0.09 cm^{-1}, respectively. The mean reduced scattering coefficients measured 16.60 $\pm$ 0.95, 14.30 $\pm$ 1.14, and 10.98 $\pm$ 2.35 cm^{-1}. The effective attenuation coefficients were calculated to be 2.00, 2.28, and 2.78 cm^{-1}, yielding OPD's of 0.5, 0.44, and 0.36 cm at 1064, 1307, and 1555 nm. ***OCT imaging studies of the prostate may benefit from replacement of commonly used 1310 nm broadband light sources with 1064 nm sources for deeper OCT imaging of the prostate.***

Table 1. Summary of canine prostate optical properties.

Coefficients (cm^{-1})	Sample No.	1064 nm	1307 nm	1555 nm
μ'_s	1	16.24	14.54	11.59
	2	16.50	14.51	9.84
	3	17.25	16.58	13.87
	4	18.10	15.57	14.44
	5	15.28	14.02	9.86
	6	17.62	14.21	12.52
	7	17.16	13.07	9.25
	8	15.86	14.38	8.55
	9	15.31	13.05	7.37
	10	16.66	13.05	12.50
	Mean	**16.60**	**14.30**	**10.98**
	σ	**0.95**	**1.14**	**2.35**
μ_a	1	0.11	0.10	0.18
	2	0.08	0.13	0.20
	3	0.06	0.07	0.20
	4	0.07	0.07	0.10
	5	0.12	0.11	0.23
	6	0.04	0.12	0.15
	7	0.03	0.22	0.24
	8	0.12	0.13	0.40
	9	0.12	0.13	0.27
	10	0.08	0.15	0.33
	Mean	**0.08**	**0.12**	**0.23**
	σ	**0.03**	**0.04**	**0.09**
μ_{eff}	**Mean**	**2.00**	**2.28**	**2.78**
OPD (cm)	**Mean**	**0.50**	**0.44**	**0.36**

B. Design OCT laparoscopic probe for prostate cancer surgery (Months 19-24).

***Objective*:** Design an OCT fiber optic probe for intraoperative guidance of laparoscopic prostate cancer surgery.

***Criteria for Success*:** Design OCT probe with 4-mm-diameter for laparoscopic prostate surgery.

Status: Not completed (This task will be worked on in Year 3 of the grant).

C. Test OCT imaging probe in an in vivo rat model (Months 19-24).

***Objective*:** Perform OCT imaging of the cavernous nerves in an in vivo rat model.

***Criteria for Success*:** Demonstrate improved discrimination of rat cavernous nerves from surrounding peri-prostatic tissues compared to preliminary studies.

Status: Completed.

Results:

A segmentation algorithm was used to locate the cavernous nerves in the prostate. An edge detection algorithm was then applied in this study to complement segmentation to provide deeper imaging of the prostate gland (Figure 3). OCT images were taken *in vivo* using a endoscopic OCT system. The OCT system was used with an 8 Fr (2.6-mm-OD) probe providing a lateral scanning distance of 2 mm and an image depth of 1.6 mm. The system was capable of acquiring real-time images with 11 *μm* axial and 25 *μm* lateral resolutions in tissue. An unprocessed TD-OCT image of the cavernous nerve at longitudinal orientation along the surface of the rat prostate is shown in Figure 3(a). Figure 3 (b) shows the combination of edge detection result of the denoised image and segmentation result. The edge detection approach was successful in accentuating prostate structures deeper in the tissue. ***The glandular structure of the prostate could be seen to a depth of approximately 1.6 mm in Figure 3(b) in comparison with an only about 1 mm depth in the unprocessed OCT image in Figure 3(a). Overall, the edge detection technique enhanced structures deeper in the prostate gland.***

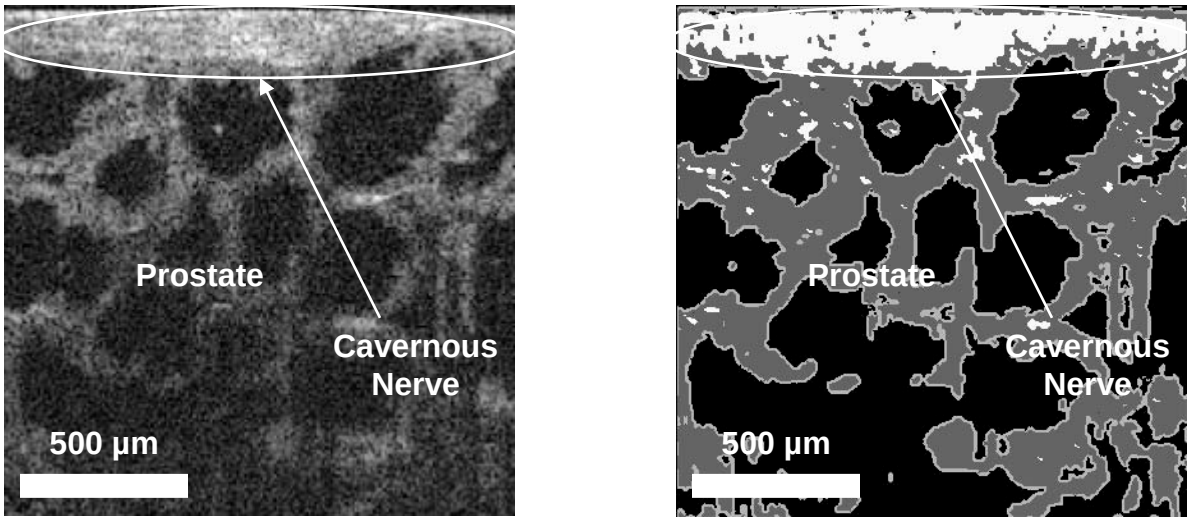

(a) (b)

Figure 3. OCT images of rat cavernous nerve: (a) Unprocessed; (b) Segmented & edge detected image.

KEY RESEARCH ACCOMPLISHMENTS

- A laparoscopic laser nerve stimulation probe was designed incorporating both laser beam collimation and beam shaping. The probe produced a collimated 1-mm-diameter spot over a working range of 20 mm. The standard Gaussian laser beam shape was also converted into a flat-top beam profile, providing more uniform irradiation of the cavernous nerve surface during stimulation. These features are significant because application of laser nerve stimulation as an intra-operative diagnostic tool during prostate cancer surgery will require delivery of a constant energy density to the nerve. Too low an energy will result in no stimulation and too high an energy will result in thermal damage to the nerve and consequent loss of erectile function. Our handheld laparoscopic probe produces a range of working distances providing constant and reproducible nerve stimulation.

- We have discovered that the threshold for laser stimulation of nerves is significantly lower than previously reported. Our research group working on the rat cavernous nerve model, as well as other research groups working on other peripheral nerve models, previously reported the threshold radiant exposure for laser nerve stimulation to be about 0.35 J/cm^2. However, using our improved flat-top laser nerve stimulation probe, we recorded successful cavernous nerve stimulation at laser radiant exposures of only 0.14 J/cm^2. This result is significant because use of a lower energy provides less probability of thermal damage to the nerve during stimulation, and also potential for use of a less expensive laser during clinical application. The flat-top probe provides much easier alignment of the laser spot with the nerve, thus producing more reliable stimulation at lower radiant exposures.

- Using our improved flat-top laparoscopic probe, we have also managed to reduce the stimulation time from 30-60 s recorded during previous studies, to less than 10 s reported during our current studies. This is significant because stimulation has to be fast and close to real-time feedback provided for the technique to be clinically viable.

- The optical properties of the prostate gland were measured for the first time at near-infrared laser wavelengths (λ = 1064, 1310, and 1550 nm) for potential use with optical coherence tomography (OCT) systems. Our study found improved optical penetration depth at 1064 nm in comparison with the conventional 1310 nm wavelength currently used in OCT. This is significant because the greatest limitation to clinical application of OCT prostate imaging is the limited imaging depth.

- We applied an image processing technique, known as segmentation, to OCT images of rat cavernous nerves and prostate, providing enhanced contrast between the two structures. We have also added edge detection to our denoising and segmentation algorithms to effectively provide deeper prostate imaging, with an improvement from approximately 1-mm depth to approximately 1.6-mm depth.

REPORTABLE OUTCOMES

Peer-Reviewed Manuscripts

Chitchian S, Weldon TP, Fried NM. Sementation of optical coherence tomography images for differentiation of the cavernous nerves from the prostate gland. Journal of Biomedical Optics 14(4):044033, 2009.

Tozburun S, Lagoda GA, Mayeh M, Farahi F, Burnett AL, Fried NM. A compact laparoscopic probe for optical stimulation of the prostate nerves. IEEE Journal of Selected Topics in Quantum Electronics. In press.

Peer-Reviewed Conference Proceedings

Chitchian S, Weldon TP, Fried NM. OCT image segmentation of the prostate nerves. Proc. SPIE 7443:74431D (San Diego, CA, 2009).

Chitchian S, Fried NM. Near-IR optical properties of canine prostate tissue using oblique incidence reflectometry. Proc. SPIE. (San Francisco, CA, 2010).

Tozburun S, Lagoda GA, Mayeh M, Burnett AL, Farahi F, Fried NM. Incorporation of fiber optic beam shaping into a laparoscopic probe for laser stimulation of the cavernous nerves. Proc. SPIE. (San Francisco, CA, 2010).

Tozburun S, Lagoda GA, Burnett AL, Fried NM. Gaussian versus flat-top spatial beam profiles for optical stimulation of the prostate nerves. Proc. SPIE. (San Francisco, CA, 2010).

Chitchian S, Fried NM. An edge detection algorithm for improving optical coherence tomography images of the prostate nerves. OSA BIOMED. (Miami, FL, 2010)

Abstracts

Chitchian S, Weldon TP, Fried NM. 2-D segmentation of OCT prostate images. Journal of Endourology 23:1031-1032, 2009.

CONCLUSION

In the second year of this project, we accomplished several tasks. First, we designed a laparoscopic laser nerve stimulation probe incorporating both laser beam collimation and shaping, resulting in more uniform irradiation of the cavernous nerve surface during stimulation. This improved probe design resulted in successful cavernous nerve stimulation at laser radiant exposures of only 0.14 J/cm^2, much lower than the threshold of 0.35 J/cm^2 previously reported. The flat-top probe provided much easier alignment of the laser spot with the nerve, thus producing more reliable stimulation at lower radiant exposures. Using our improved flat-top laparoscopic probe, we also reduced the stimulation time from 30 s recorded during previous studies, to less than 10 s reported during our current studies, thus faster stimulation necessary for real-time application in the clinic. The optical properties of the prostate gland were also measured for the first time at near-infrared laser wavelengths commonly used with optical coherence tomography (OCT) systems. Our study found improved optical penetration depth at 1064 nm in comparison with the conventional 1310 nm wavelength currently used in OCT. Finally, we also combined the application of several image processing algorithms (denoising, segmentation, and edge detection) to optical coherence tomography images of the rat prostate and cavernous nerves to improve the signal to noise ratio, contrast to noise ratio, and imaging depth. Overall, during Year 2 of the grant, we published 2 manuscripts, 5 conference proceedings, and 1 abstract. Our research results were also presented at several national and international conferences, including the International Symposium for Biomedical Optics (SPIE), the Engineering and Urology Society (EUS) annual meeting, and the Optical Society of America (OSA) Biomedical Symposium.

REFERENCES

1. G. P. Murphy, C. Mettlin, H. Menck, D. P. Winchester, and A. M. Davidson, "National patterns of prostate cancer treatment by radical prostatectomy: results of a survey by the American College of Surgeons Committee on Cancer," *J. Urol.*, vol. 152, 1817-1819, 1994.
2. J. A. Talcott, P. Rieker, K. J. Propert, J. A. Clark, K. I. Wishnow, K. R. Loughlin, J. P. Richie, and P. W. Kantoff, "Patient-reported impotence and incontinence after nerve-sparing radical prostatectomy," *J. Natl. Cancer Inst.*, vol. 89, pp. 1117-1123, 1997.
3. V. E. Weldon, F. R. Tavel, and H. Neuwirth, Continence, potency and morbidity after radical perineal prostatectomy," *J. Urol.*, vol. 158:1470-1475, 1997.
4. W. J. Catalona, G. F. Carvalhal, D. E. Mager, and D. S. Smith, "Potency, continence and complication rates in 1,870 consecutive radical retropubic prostatectomies," *J. Urol.*, vol. 162, pp. 433-438, 1999.
5. P. C. Walsh, P. Marschke, D. Ricker, and A. L. Burnett, "Patient-reported urinary continence and sexual function after anatomic radical prostatectomy," *Urol.*, vol. 55, pp. 58-61, 2000.
6. A. L. Burnett, G. Aus, E. D. Canby-Hagino, M. S. Cookson, A. V. D'Amico, R. R. Dmochowski, D. T. Eton, J. D. Forman, S. L. Goldenberg, J. Hernandez, C. S. Higano, S. Kraus, M. Liebert, J. W. Moul, C. Tangen, J. B. Thrasher, I. Thompson, "Erectile function outcome reporting after clinically localized prostate cancer treatment," *J. Urol.*, vol. 178(2), pp. 597-601, 2007.
7. A. J. Costello, M. Brooks, and O. J. Cole, "Anatomical studies of the neurovascular bundle and cavernosal nerves," *BJU Int.*, vol. 94, pp. 1071-1076, 2004.
8. N. M. Fried, S. Rais-Bahrami, G. A. Lagoda, Y. Chuang, A. L. Burnett, and L. M. Su, "Imaging the cavernous nerves in the rat prostate using optical coherence tomography," *Lasers Surg. Med.*, vol. 39, pp. 36-41, 2007.
9. D. Huang, E. A. Swanson, C. P. Lin, J. S. Schuman, W. G. Stinson, W. Chang, M. R. Hee, T. Flotte, K. Gregory, C. A. Puliafito, and J. G. Fujimoto, "Optical coherence tomography," *Science*, vol. 254, pp. 1178-1181, 1991.
10. G. J. Tearney, M. E. Brezinski, B. E. Bouma, S. A. Boppart, C. Pitris, J. F. Southern, and J. G. Fujimoto, "In vivo endoscopic optical biopsy with optical coherence tomography," *Science*, vol. 276, pp. 2037-2039, 1997.
11. F. Koenig, G. J. Tearney, and B. E. Bouma, "Optical coherence tomography in urology," Ch. 28, In Handbook of Optical Coherence Tomography, Eds. B. E. Bouma and G. J. Tearney, Marcel Dekker: New York, 2002.
12. P. Crow, N. Stone, C. A. Kendall, R. A. Persad, and M. P. Wright, "Optical diagnostics in urology: current applications and future prospects," *BJU Int.*, vol. 92, pp. 400-407, 2003.
13. G. J. Tearney, M. E. Brezinski, J. F. Southern, B. E. Bouma, S. A. Boppart, and J. G. Fujimoto, "Optical biopsy in human urologic tissue using optical coherence tomography," *J. Urol.*, vol. 157, pp. 1915-1919, 1997.
14. A. V. D'Amico, M. Weinstein, X. Li, J. P. Richie, and J. Fujimoto, "Optical coherence tomography as a method for identifying benign and malignant microscopic structures in the prostate gland," *Urol.*, vol. 55, pp. 783-787, 2000.
15. S. A. Boppart, J. M. Herrmann, C. Pitris, D. L. Stamper, M. E. Brezinski, and J. G. Fujimoto, "Real-time optical coherence tomography for minimally invasive imaging of prostate ablation," *Comput. Aided Surg.*, vol. 6, pp. 94-103, 2001.
16. L. Klotz, "Neurostimulation during radical prostatectomy: improving nerve-sparing techniques," *Semin. Urol. Oncol.*, vol. 18, pp. 46-50, 2000.
17. H. L. Kim, D. S. Stoffel, D. A. Mhoon, and C. B. Brendler, "A positive caver map response poorly predicts recovery of potency after radical prostatectomy," *Urol.*, vol. 56, pp. 561-564, 2000.

18. L. Klotz, J. Heaton, M. Jewett, J. Chin, N. Fleshner, L. Goldenberg, and M. Gleave, "A randomized phase 3 study of intraoperative cavernous nerve stimulation with penile tumescence monitoring to improve nerve sparing during radical prostatectomy," *J. Urol.*, vol. 164, pp. 1573-1578, 2000.
19. J. Holzbeierlein, M. Peterson, and J. A. Smith Jr, "Variability of results of cavernous nerve stimulation during radical prostatectomy," *J. Urol.*, vol. 165, pp. 108-110, 2001.
20. P. C. Walsh, P. Marschke, W. J. Catalona, H. Lepor, S. Martin, R. P. Myers, and M. S. Steiner, "Efficacy of first-generation Cavermap to verify location and function of cavernous nerves during radical prostatectomy: a multi-institutional study by experienced surgeons," *Urol.*, vol. 57, pp. 491-494, 2001.
21. H. L. Kim, D. A. Mhoon, and C. B. Brendler, "Does the CaverMap device help preserve potency?" *Curr. Urol. Rep.*, vol. 2, pp. 214-217, 2001.
22. L. Klotz, "Cavernosal nerve mapping: current data and applications," *BJU Int.*, vol. 93, pp. 9-13, 2004.
23. J. Wells, C. Kao, K. Mariappan, J. Albea, E. D. Jansen, P. Konrad, and A. Mahadevan-Jansen, "Optical stimulation of neural tissue in vivo," *Opt. Lett.*, vol. 30, pp. 504-506, 2005.
24. J. Wells, C. Kao, E. D. Jansen, P. Konrad, and A. Mahadevan-Jansen, "Application of infrared light for in vivo neural stimulation," *J. Biomed. Opt.*, vol. 10:064003, pp. 1-11, 2005.
25. A. D. Izzo, C. P. Richter, E. D. Jansen, and J. T. Walsh, "Laser stimulation of the auditory nerve," *Lasers Surg. Med.*, vol. 38, pp. 745-753, 2006.
26. A. D. Izzo, J. T. Walsh, E. D. Jansen, M. Bendett, J. Webb, H. Ralph, and C. P. Richter, "Optical parameter variability in laser nerve stimulation: a study of pulse duration, repetition rate, and wavelength," *IEEE Trans. Biomed. Eng.*, vol. 54, pp. 1108-1114, 2007.
27. J. D. Wells, S. Thomsen S, P. Whitaker, E. D. Jansen, C. C. Kao, P. E. Konrad, A. Mahadevan-Jansen, "Optical mediated nerve stimulation: identification of injury thresholds," *Lasers Surg. Med.* vol. 39, pp. 513-526, 2007.
28. J. Bush, P. Davis, and M. A. Marcus, "All-fiber optic coherence domain interferometric techniques," *Proc. SPIE*, vol. 4204A-08, 2000.
29. F. Feldchtein, J. Bush J, G. Gelikonov, V. Gelikonov, and S. Piyevsky S, "Cost-effective, all-fiber autocorrelator based 1300 nm OCT system," *Proc. SPIE*, vol. 5690, pp. 349-354, 2005.
30. U. Sharma, N. M. Fried, and J. U. Kang, "All-fiber common-path optical coherence tomography: sensitivity optimization and system analysis," *IEEE J. Sel. Top. Quant. Electron.*, vol. 11, pp. 799-805, 2005.
31. F. Feldchtein, N. Tresser, M. Kareta, D. Bodner, I. Gill, J. Kaouk, P. Kick, G. MacLennan, W. Kuang, L. Schoenfeld, E. Klein, M. Resnick, "Niris optical coherence tomography system: principle of operation and applications in endourology," *J. Endourol.*, vol. 20 (Suppl 1):A198, 2006.
32. M. Aron, J. H. Kaouk, N. J. Hegarty, J. R. Colombo, Jr., G. P. Haber, B. I. Chung, M. Zhou, I. S. Gill, "Preliminary experience with the Niris optical coherence tomography system during laparoscopic and robotic prostatectomy," *J. Endourol.*, vol. 21(8), pp. 814-818, 2007.

APPENDIX

Peer-Reviewed Manuscripts

Chitchian S, Weldon TP, Fried NM. Sementation of optical coherence tomography images for differentiation of the cavernous nerves from the prostate gland. Journal of Biomedical Optics 14(4):044033, 2009.

Tozburun S, Lagoda GA, Mayeh M, Farahi F, Burnett AL, Fried NM. A compact laparoscopic probe for optical stimulation of the prostate nerves. IEEE Journal of Selected Topics in Quantum Electronics. In press.

Peer-Reviewed Conference Proceedings

Chitchian S, Weldon TP, Fried NM. OCT image segmentation of the prostate nerves. Proc. SPIE 7443:74431D (San Diego, CA, 2009).
2009.

Chitchian S, Fried NM. Near-IR optical properties of canine prostate tissue using oblique incidence reflectometry. Proc. SPIE 7548:75480Z (San Francisco, CA, 2010).

Tozburun S, Lagoda GA, Mayeh M, Burnett AL, Farahi F, Fried NM. Incorporation of fiber optic beam shaping into a laparoscopic probe for laser stimulation of the cavernous nerves. Proc. SPIE 7548:754818 (San Francisco, CA, 2010).

Tozburun S, Lagoda GA, Burnett AL, Fried NM. Gaussian versus flat-top spatial beam profiles for optical stimulation of the prostate nerves. Proc. SPIE 7548:75484W (San Francisco, CA, 2010).

Chitchian S, Fried NM. An edge detection algorithm for improving optical coherence tomography images of the prostate nerves. OSA BIOMED. (Miami, FL, 2010).

Abstracts

Chitchian S, Weldon TP, Fried NM. 2-D segmentation of OCT prostate images. Journal of Endourology 23:1031-1032, 2009.

Segmentation of optical coherence tomography images for differentiation of the cavernous nerves from the prostate gland

Shahab Chitchian
University of North Carolina at Charlotte
Department of Physics and Optical Science
9201 University City Boulevard
Charlotte, North Carolina 28223

Thomas P. Weldon
University of North Carolina at Charlotte
Department of Electrical and Computer Engineering
9201 University City Boulevard
Charlotte, North Carolina 28223

Nathaniel M. Fried
University of North Carolina at Charlotte
Department of Physics and Optical Science
9201 University City Boulevard
Charlotte, North Carolina 28223
and
Johns Hopkins Medical Institutions
Department of Urology
600 North Wolfe Street
Baltimore, Maryland 21287

Abstract. The cavernous nerves course along the surface of the prostate and are responsible for erectile function. Improvements in identification, imaging, and visualization of the cavernous nerves during prostate cancer surgery may improve nerve preservation and postoperative sexual potency. Two-dimensional (2-D) optical coherence tomography (OCT) images of the rat prostate were segmented to differentiate the cavernous nerves from the prostate gland. To detect these nerves, three image features were employed: Gabor filter, Daubechies wavelet, and Laws filter. The Gabor feature was applied with different standard deviations in the *x* and *y* directions. In the Daubechies wavelet feature, an 8-tap Daubechies orthonormal wavelet was implemented, and the low-pass sub-band was chosen as the filtered image. Last, Laws feature extraction was applied to the images. The features were segmented using a nearest-neighbor classifier. *N*-ary morphological postprocessing was used to remove small voids. The cavernous nerves were differentiated from the prostate gland with a segmentation error rate of only 0.058 ± 0.019. This algorithm may be useful for implementation in clinical endoscopic OCT systems currently being studied for potential intraoperative diagnostic use in laparoscopic and robotic nerve-sparing prostate cancer surgery. [DOI: 10.1117/1.3210767]

Keywords: segmentation; optical coherence; tomography; cavernous nerves; prostate; prostatectomy; CT.

Paper 09065R received Feb. 25, 2009; revised manuscript received Jun. 12, 2009; accepted for publication Jun. 23, 2009; published online Aug. 25, 2009.

1 Introduction

Preservation of the cavernous nerves during prostate cancer surgery is critical in preserving a man's ability to have spontaneous erections following surgery. These microscopic nerves course along the surface of the prostate within a few millimeters of the prostate capsule, and they vary in size and location from one patient to another, making preservation of the nerves difficult during dissection and removal of a cancerous prostate gland. These observations may explain in part the wide variability in reported potency rates (9 to 86%) following prostate cancer surgery.[1] Any technology capable of providing improved identification, imaging, and visualization of the cavernous nerves during prostate cancer surgery would be of great assistance in increasing sexual function rates after surgery.

Optical coherence tomography (OCT) is a noninvasive optical imaging technique used to perform high-resolution cross-sectional *in vivo* and *in situ* imaging of microstructure in biological tissues.[2] OCT imaging of the cavernous nerves in the rat and human prostate has recently been demonstrated.[3–5] However, further improvement in the quality of the images is necessary before OCT can be used in the clinic as an intraoperative diagnostic tool during nerve-sparing prostate cancer surgery.

Three-dimensional (3-D) prostate segmentation, which allows clinicians to design an accurate brachytherapy treatment plan for prostate cancer, has been previously reported using computed tomography (CT), magnetic resonance imaging (MRI), and ultrasound.[6,7] Recently, various segmentation approaches have also been applied in retinal OCT imaging. Ishikawa et al. described an approach to segment retinal layers and extract thickness of the layers.[8] Their algorithm searches for borders of retinal layers by applying an adaptive thresholding technique. Bagci et al. described an algorithm to detect layers within the retinal tissue by enhancing edges along the image vertical dimension.[9] Methods based on a Markov model and deformable splines were reported for determination of optic nerve-head geometry and thickness of retinal nerve fibers, respectively.[10,11] However, large irregular voids in prostate OCT images require a segmentation approach different than that used for segmentation of the more regular structure of retinal layers.

Our research group recently applied the wavelet shrinkage denoising technique to improve the quality of OCT images of

Address all correspondence to: Shahab Chitchian, Department of Physics and Optical Science, University of North Carolina at Charlotte, Charlotte, NC 28223. Tel: 704-687-8152; Fax: 704-687-8197; E-mail: schitchi@uncc.edu

1083-3668/2009/14(4)/044033/4/$25.00 © 2009 SPIE

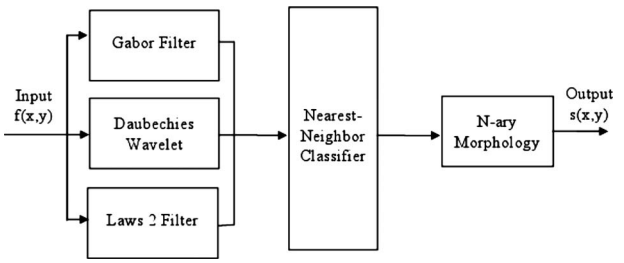

Fig. 1 System block diagram. Input image $f(x,y)$ is processed into three feature images: Gabor filtered image, 8-tap Daubechies wavelet sub-band, and Laws feature. The features are classified by a *k*-nearest neighbors classifier into three classes: background, nerve, and prostate gland. Last, *N*-ary morphological close and open functions are applied, generating the final output segmented image $s(x,y)$.

the prostate for identification of the cavernous nerves.[12] Building on these earlier results, the segmentation technique reported here has the advantage that it is not dependent on the depth of the nerves below the tissue surface. In this regard, the proposed segmentation approach is a more versatile method. In this study, 2-D prostate images are segmented into three regions of background, nerve, and prostate gland using a nearest-neighbor classifier.

2 Segmentation System

A block diagram of the segmentation system is provided in Fig. 1. The input image $f(x,y)$ is first processed to form three feature images. The features are generated by Gabor filtering, Daubechies wavelet transform, and Laws filter mask, respectively. The prostate image is then segmented into nerve, prostate, and background classes using a *k*-nearest neighbors classifier and the three feature images. Last, *N*-ary morphological postprocessing is used to remove small voids. The generation of the feature images are first described here, followed by descriptions of the classifier and postprocessing.

2.1 *Gabor Filter*

The first feature image is generated by a Gabor filter with impulse response $h(x,y)$,[13]

$$h(x,y) = g(x,y)\exp[-j2\pi(Ux + Vy)], \tag{1}$$

where

$$g(x,y) = \frac{1}{2\pi\sigma_x\sigma_y}\exp\left[-\frac{1}{2}\left(\frac{x^2}{\sigma_x^2} + \frac{y^2}{\sigma_y^2}\right)\right]. \tag{2}$$

The Gabor function $h(x,y)$ is a complex sinusoid centered at frequency (U,V) and modulated by a Gaussian envelope $g(x,y)$. The spatial extent of the Gaussian envelope is determined by parameters σ_x,σ_y. The 2-D Fourier transform of $h(x,y)$ is

$$H(u,v) = G(u - U, v - V), \tag{3}$$

where

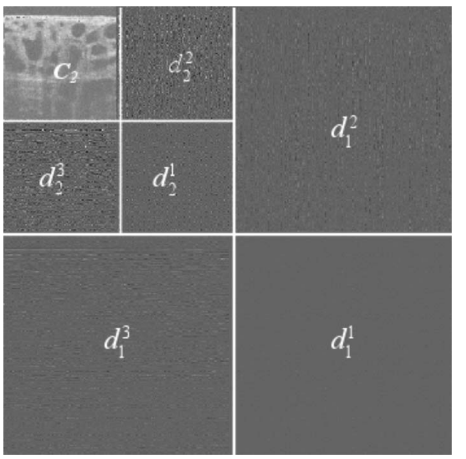

Fig. 2 Ordering of the approximation and detail coefficients of a two-level 2-D wavelet transform.

$$G(u,v) = \exp[-2\pi^2(\sigma_x^2u^2 + \sigma_y^2v^2)], \tag{4}$$

is the Fourier transform of $g(x,y)$. The parameters (U,V,σ_x,σ_y) determine $h(x,y)$. Equations (3) and (4) show that the Gabor function is essentially a bandpass filter centered about frequency (U,V) with bandwidth determined by σ_x,σ_y. The Gabor feature center frequency of $(0.2,0.2)$ cycles/pixel is applied with standard deviations of 3 and 6 in the x and y directions, respectively, based on experimental observation of minimum segmentation error.

2.2 *Daubechies Wavelet Transform*

The second feature is generated by an 8-tap Daubechies orthonormal wavelet transform, which is the representation of a function by scaled and translated copies of a finite-length or fast-decaying oscillating wave form that can be used to analyze signals at multiple scales. Wavelet coefficients carry both time and frequency information, as the basis functions vary in position and scale.

The discrete wavelet transform (DWT) converts a signal to its wavelet representation. In a one-level DWT, the image c_0 is split into an approximation part c_1 and a detail part d_1. In a multilevel DWT, each subsequent c_i is split into an approximation c_{i+1} and detail d_{i+1}. For 2-D images, each c_i is split into an approximation c_{i+1} and three detail channels d_{i+1}^1, d_{i+1}^2 and d_{i+1}^3 for horizontally, vertically, and diagonally oriented details, respectively, as illustrated in Fig. 2. The inverse DWT (IDWT) reconstructs each c_i from c_{i+1} and d_{i+1}. In the present work, the approximation part c_1 is chosen as the filtered image for the second feature.

2.3 *Laws Filter*

The third feature is generated by the Laws feature extraction method. The set of nine Laws 3×3 pixel impulse response arrays $h_i(x,y)$ (Ref. 14) is convolved with a texture field to accentuate its microstructure. The i'th microstructure image $m_i(x,y)$ is defined as

$$m_i(x,y) = f(x,y) * h_i(x,y). \tag{5}$$

Then, the energy of these microstructure arrays is measured by forming their moving window standard deviation $T_i(x,y)$ according to

$$T_i(x,y) = \frac{1}{2w+1}\left\{ \sum_{m=-w}^{w} \sum_{n=-w}^{w} [m_i(x+m,y+n) - \mu(x+m,y+n)]^2 \right\}^{1/2}, \quad (6)$$

where w sets the window size, and $\mu(x,y)$ is the mean value of $m_i(x,y)$ over the window.

For the present system, Laws feature extraction is applied by using the Laws 2 mask as follows:

$$Laws2 = \frac{1}{12}\begin{pmatrix} 1 & 0 & -1 \\ 2 & 0 & -2 \\ 1 & 0 & -1 \end{pmatrix}. \quad (7)$$

Standard deviation computation of Eq. (6) is performed after the Laws mask filtering to complete the Laws feature extraction.

2.4 *K-Nearest Neighbors Classifier*

The k-nearest neighbors algorithm (k-NN) is a method for classifying objects where classification is based on the k-closest training samples in the feature space. It is implemented by the following steps:

1. **Training:** The training phase of the algorithm consists only of storing the feature vectors and class labels of the training samples. The space is partitioned into regions by locations and labels of the training samples. Three classes are used: background, nerve, and prostate gland.
2. **Parameter selection:** The best choice of the parameter k depends on the data, where larger values of k typically reduce the effect of noise on the classification but make boundaries between classes less distinct. A parameter value of $k=10$ is empirically chosen (k varied from 4 to 12) for the present implementation of the k-nearest neighbors algorithm for segmentation of the prostate images.
3. **Classification scheme:** After training the classifier and selecting the parameter k, the prostate image is segmented based on the three feature images forming the feature vector. The Euclidean distances from the image feature vector to all stored vectors are computed, and the k-closest samples are selected. A point in the prostate image is assigned to the nerve class if it is the most frequent class label among the k-nearest training samples. After classification, the N-ary morphological postprocessing is applied to remove small voids in the final results.

2.5 *N-ary Morphological Postprocessing*

The N-ary morphological postprocessing method for eliminating small misclassified regions proceeds in two steps.[15] In the first step, pixels whose neighborhood consists entirely of one class in the classified image are left unchanged. Otherwise, the pixel value is set to zero to indicate that the pixel is no longer assigned to any class. In the second step, each unassigned pixel is assigned to the most prevalent class within the 8-neighborhood surrounding the pixel.

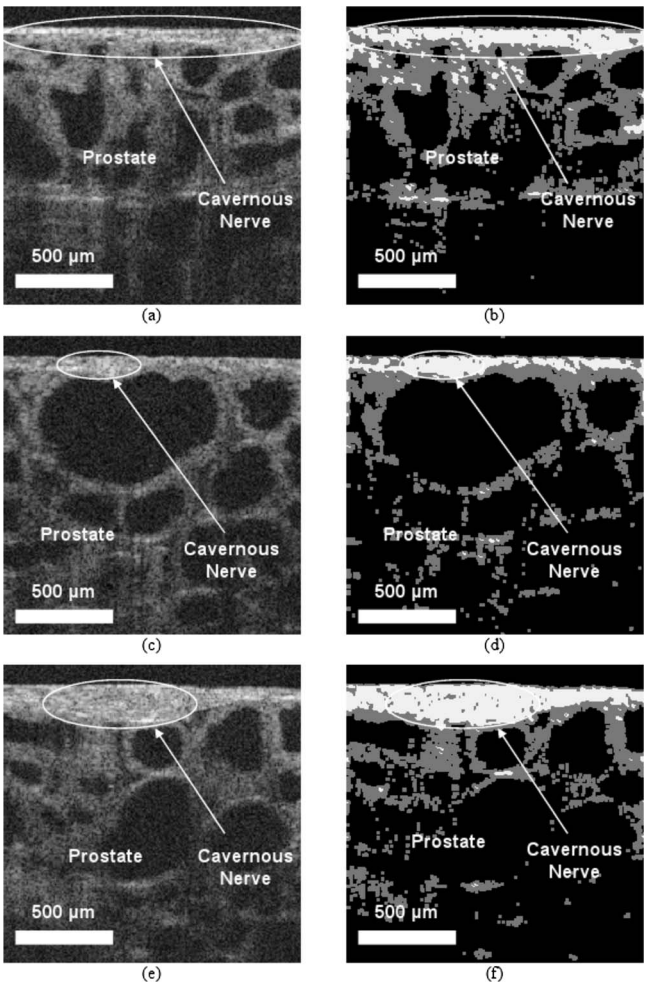

Fig. 3 OCT images of the rat cavernous nerve: (a) and (b) longitudinal section; (c) and (d) cross section; (e) and (f) oblique section. (a), (c), and (e) Before; and (b), (d), and (f) after segmentation.

3 Results

OCT images were taken *in vivo* in a rat model using a clinical endoscopic OCT system (Imalux, Cleveland, Ohio) based on an all single-mode fiber (SMF) common-path interferometer-based scanning system (Optiphase, Van Nuys, California). Mathcad 14.0 (Parametric Technology Corporation, Needham, Massachusetts) was used for implementation of the segmentation algorithm described earlier.

Figures 3(a), 3(c), and 3(e) show the original OCT images of the cavernous nerves at different orientations (longitudinal, cross-sectional, and oblique) coursing along the surface of the rat prostate. Figures 3(b), 3(d), and 3(f) show the same OCT images after segmentation using the system of Fig. 1. The cavernous nerves could be differentiated from the prostate gland using this segmentation algorithm.

The error rate was calculated by: Error=(No. of error pixels)/(No. of total pixels), where (No. of error pixels)=(No. of false-positives+No. of false-negatives). The overall error rate for the segmentation was 0.058 with a standard deviation of 0.019, indicating the robustness of our technique. The error rate was measured as a mean of error measurements for three different sample images at different orientations (longitudinal,

cross-sectional, and oblique). A different image was used for training. The error rate was determined by comparing manually segmented images to the automatically segmented images. These manually segmented images of the cavernous nerves were previously created according to histologic correlation with OCT images.[12]

Overall, the proposed image segmentation of Fig. 1 performed well for identification of the cavernous nerves in the prostate. Areas that need improvement include the classification of prostate gland in which there are a few small scattered regions (shown in white) in the prostate that are erroneously segmented as part of the nerves [e.g., Fig. 3(b)]. For the present study, it was advantageous to manually vary the Gabor filter parameters so that the Gabor filter efficacy could be directly observed in the filtered images. Based on prior investigations,[13,16] the present results demonstrate the potential of our overall approach, although future work could include automation of Gabor filter parameter selection. Cross-validation, parameter optimization, and evaluation of alternative classifiers could also be performed. Nevertheless, our current results provide a foundation for more comprehensive studies.

Last, it should be noted that the rat model represents an idealized version of the prostate anatomy because the cavernous nerve lies on the surface of the prostate and is therefore directly visible. However, in the human anatomy, there may be intervening tissue between the OCT probe and the nerves, making identification more difficult. An important advantage of the proposed classifier-based segmentation approach is that the classifier should also be able to locate the cavernous nerve when it lies at various depths beneath the surface.

4 Conclusion

This algorithm for image segmentation of the prostate nerves may prove useful for implementation in clinical endoscopic OCT systems currently being studied for use in laparoscopic and robotic nerve-sparing prostate cancer surgery.

Acknowledgments

This research was supported by the Department of Defense Prostate Cancer Research Program, Grant No. PC073709. The authors thank Nancy Tresser of Imalux Corporation (Cleveland, Ohio) for lending us the Niris OCT system for these studies.

References

1. A. Burnett, G. Aus, E. Canby-Hagino, M. Cookson, A. D'Amico, R. Domchowski, D. Eton, J. Forman, S. Goldenberg, J. Hernandez, C. Higano, S. Kraus, M. Liebert, J. Moul, C. Tangen, J. Thrasher, and I. Thompson, "Function outcome reporting after clinically localized prostate cancer treatment," *J. Urol.* **178**, 597–601 (2007).
2. D. Huang, E. Swanson, C. Lin, J. Schuman, W. Stinson, W. Chang, M. Hee, T. Flotte, K. Gregory, C. Puliafito, and J. Fujimoto, "Optical coherence tomography," *Science* **254**, 1178–1181 (1991).
3. M. Aron, J. Kaouk, N. Hegarty, J. Colombo, G. Haber, B. Chung, M. Zhou, and I. Gill, "Preliminary experience with the niris optical coherence tomography system during laparoscopic and robotic prostatectomy," *J. Endourol.* **21**, 814–818 (2007).
4. N. Fried, S. Rais-Bahrami, G. Lagoda, A. Chuang, A. Burnett, and L. Su, "Imaging the cavernous nerves in rat prostate using optical coherence tomography," *Lasers Surg. Med.* **39**, 36–41 (2007).
5. S. Rais-Bahrami, A. Levinson, N. Fried, G. Lagoda, A. Hristov, A. Chuang, A. Burnett, and L. Su, "Optical coherence tomography of cavernous nerves: a step toward real-time intraoperative imaging during nerve-sparing radical prostatectomy," *Urology* **72**, 198–204 (2008).
6. D. Freedman, R. Radke, T. Zhang, Y. Jeong, D. Lovelock, and G. Chen, "Model-based segmentation of medical imagery by matching distributions," *IEEE Trans. Med. Imaging* **24**, 281–292 (2005).
7. Y. Zhan and D. Shen, "Deformable segmentation of 3-D ultrasound prostate images using statistical texture matching method," *IEEE Trans. Med. Imaging* **25**, 256–272 (2006).
8. H. Ishikawa, D. Stein, G. Wollstein, S. Beaton, J. Fujimoto, and J. Schuman, "Macular segmentation with optical coherence tomography," *Invest. Ophthalmol. Visual Sci.* **46**, 2012–2017 (2005).
9. A. Bagci, R. Ansari, and M. Shahidi, "A method for detection of retinal layers by optical coherence tomography image segmentation," in *Proc. 3rd Life Science Systems and Applications Workshop (LISSA 2007)*, 8–9 November 2007, Bethesda, MD, p. 144, IEEE, Piscataway, NJ (2007).
10. K. Boyer, A. Herzog, and C. Roberts, "Automatic recovery of the optic nervehead geometry in optical coherence tomography," *IEEE Trans. Med. Imaging* **25**, 553–570 (2006).
11. M. Mujat, R. Chan, B. Cense, B. Park, C. Joo, T. Akkin, T. Chen, and J. de Boer, "Retinal nerve fiber layer thickness map determined from optical coherence tomography images," *Opt. Express* **13**, 9480–9491 (2005).
12. S. Chitchian, M. Fiddy, and N. Fried, "Denoising during optical coherence tomography of the prostate nerves via wavelet shrinkage using dual-tree complex wavelet transform," *J. Biomed. Opt.* **14**, 014031 (2009).
13. T. Weldon, W. Higgins, and D. Dunn, "Efficient Gabor filter design for texture segmentation," *Pattern Recogn.* **29**, 2005–2015 (1996).
14. W. Pratt, *Digital Image Processing*, Wiley, Hoboken. NJ (2007).
15. T. Weldon, "Removal of image segmentation boundary errors using an *N*-ary morphological operator," in *Proc. IEEE Southeast Conf.*, March 22–25, 2007, Richmond, VA , p. 509, IEEE, Piscataway, NJ (2007).
16. T. Weldon and W. Higgins, "Designing multiple Gabor filters for multitexture image segmentation," *Opt. Eng.* **38**, 1478–1489 (1999).

A Compact Laparoscopic Probe for Optical Stimulation of the Prostate Nerves

Serhat Tozburun[1], Mona Mayeh[1], Gwen A. Lagoda[2],
Faramarz Farahi[1], Arthur L. Burnett[2], and Nathaniel M. Fried[1,2]

[1] Department of Physics and Optical Science, University of North Carolina at Charlotte, NC
[2] Department of Urology, Johns Hopkins Medical Institutions, Baltimore, MD

***Abstract* – The cavernous nerves course along the prostate surface and are responsible for sexual function. Optical nerve stimulation has recently been tested as a potential alternative to electrical nerve stimulation for identifying and preserving these delicate nerves during prostate cancer surgery. However, the optimal range of laser parameters for safe and consistent laser nerve stimulation is relatively narrow: low level irradiation may not stimulate the nerve, while high level irradiation may result in thermal damage to the nerve and loss of erectile function. The objective of this study is to design, build and provide preliminary data on testing of a laparoscopic probe capable of delivering a collimated, flat-top spatial beam profile to the nerve surface for uniform, safe, and reproducible irradiation of the nerve. Chemical etching of the distal fiber optic tip in combination with an aspheric lens resulted in a 3.4-mm-outer-diameter laparoscopic probe capable of delivering a collimated, 1-mm-diameter, flat-top laser beam over a working distance of about 20 mm. Successful optical nerve stimulation using this probe was observed in a rat prostate model, *in vivo*. Upon further testing, this probe may be useful for identifying and preserving the cavernous nerves during laparoscopic nerve-sparing prostate cancer surgery.**

***Index Terms* – laser biomedical applications, thulium, nervous system, urinary system**

I. INTRODUCTION AND BACKGROUND

A. Cavernous Nerves (CN)

Preservation of the cavernous nerves (CN) during prostate cancer surgery is critical in preserving a man's ability to have spontaneous erections following surgery. Because of the close proximity of the nerves to the prostate surface, they are at risk of injury during dissection and removal of a cancerous prostate gland. Their microscopic nature also makes it difficult to predict the location and path of these nerves from one patient to another. These observations may, in part, explain the wide variability in reported sexual potency rates (9-86%) following prostate cancer surgery [1]. Recent anatomic studies also suggest that the CN may have more extensive branching along the prostate surface than originally thought, and that our current understanding of the location, extent, and course of these nerves may be limited [2]. Improvements in identification of the CN during surgery would aid preservation of the nerves and improve post-operative sexual function, resulting in direct patient benefit.

Our laboratory is currently studying optical nerve stimulation as a potential intra-operative diagnostic tool for improved identification of the CN. The rat prostate serves as an excellent small animal model for preliminary study of the CN, as the rat CN is a large, visible, and distinct bundle allowing for easy identification.

B. Electrical Nerve Stimulation (ENS)

Conventional Electrical Nerve Stimulation (ENS) of the CN is currently used in scientific studies to measure erectile response. Intra-operative nerve mapping devices have also been used as surgical diagnostic tools to assist in preservation of the CN during nerve-sparing prostate cancer surgery [3]. However, these nerve mapping technologies have proven inconsistent and unreliable in identifying the CN and evaluating nerve function [4-8].

Electrical nerve stimulation has several general limitations. First, ENS is limited by the need for physical contact between the electrode and the tissue, which may result in tissue damage. Second, the spatial precision of ENS is limited by the electrode's size. Third, ENS produces artifacts that may interfere with measurement.

C. Optical Nerve Stimulation (ONS)

Recently, Optical Nerve Stimulation (ONS) has been demonstrated using pulsed infrared lasers [9-13]. ONS offers several advantages over ENS, including: (1) a non-contact method of stimulation, (2) improved spatial selectivity, and (3) elimination of stimulation artifacts.

Our laboratory has previously reported successful ONS of the CN in a rat model, in vivo [14-16]. We are currently developing this technique as a potential intra-operative diagnostic method for identifying and preserving the CN during laparoscopic and robotic prostatectomy. However, one limitation of this technique is that there is a relatively narrow range of parameters for nerve stimulation: a fluence less than ~ 0.35 J/cm^2 does not produce a reliable response, while a fluence above ~ 0.6-1.0 J/cm^2 results in nerve

damage upon repetitive stimulation [13,14]. Since the fluence at the fiber output end may decrease rapidly due to beam divergence, it is critical that the probe produce a collimated beam over a short working distance (e.g. several millimeters), so that a constant fluence corresponding to safe and reproducible stimulation can be achieved. The nerve is a delicate tissue structure, so it may also be important that a flat-top beam profile be used to provide a uniform fluence across the nerve surface, and further avoid potential heat-induced nerve damage during laser stimulation.

Preliminary work in our laboratory demonstrated that a collimated beam could be produced within the confines of a laparoscopic probe design [17]. This study extends this work further to include fiber optic beam shaping methods for converting the Gaussian beam profile to a flat-top beam profile. The objective of this study is two-fold: (1) to describe the design of a laparoscopic probe capable of delivering a small, collimated, flat-top beam over a short distance, and (2) to describe the preliminary testing of the probe in a rat cavernous nerve model, *in vivo*.

II. MATERIALS AND METHODS

A. Fiber Optic Beam Shaping

A 200-μm-core, low-OH silica fiber with 0.22 NA (BFL22-200, Thorlabs, Newton, NJ), was used in these studies. The core of the distal fiber tip was chemically etched with hydrofluoric acid (HFA) for 1 min at room temperature and then cleaned with distilled (DI) water. During the etching process, the fiber was surrounded by 49% HFA diluted with DI water in a 1:4 ratio (acid/water). The central 100 μm of the fiber tip was chemically etched to a depth of approximately 2 μm.

Computer simulations using fiber optic ray tracing software (RSoft Photonics CAD Suite Version 8.0.1., Ossining, NY), based on advanced finite difference beam propagation techniques, were used to help optimize the chemical etching conditions necessary to provide a flat-top spatial beam profile.

B. Laparoscopic Probe Design

The laparoscopic probe consisted of several components (Figure 1). A standard probe from an existing disposable laparoscopic instrument was used to house a miniature linear motorized stage (MM-3M-F-1, National Aperture, Salem, NH), capable of scanning a distance of 25 mm for side-firing delivery. The motorized stage was connected to a PC via USB connections and operated with Labview software. A 30-cm-long, stainless steel rod (2.7-mm-ID, 3.4-mm-OD, HTX-10R-24-05, Small Parts, Miami Lakes, FL), capable of being inserted through a standard 5-mm-ID laparoscopic port was attached to the stage. This rod housed the optics inside a quartz capillary tube (2.0-mm-ID, 2.4-mm-OD, CV2024, Vitrocom, Mountain Lakes, NJ). The optics consisted of an aspheric lens (2-mm-OD, 350430-C, Thorlabs) and a 45° rod mirror (2-mm-OD, NT54-091, Edmund Optics, Barrington, NJ) with custom gold coating (International Micro Photonix, Tewksbury, MA). The optical fiber was inserted into a glass ferrule (Vitrocom) for centering with the optics, and then glued into place inside the glass capillary tubing.

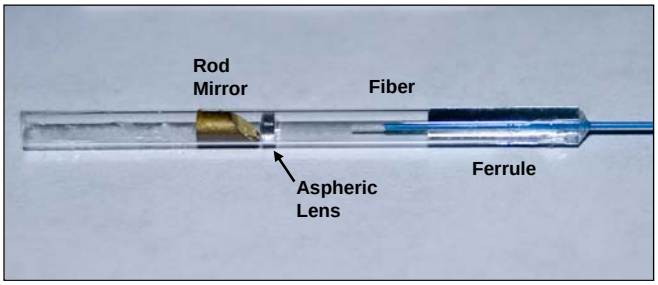

(a)

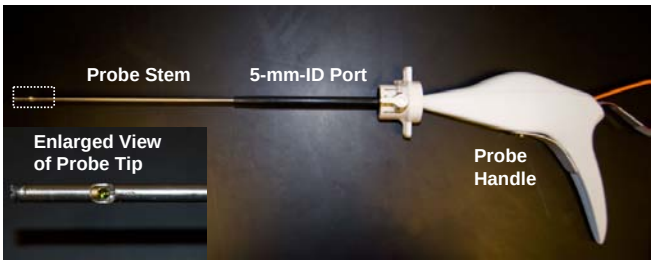

(b)

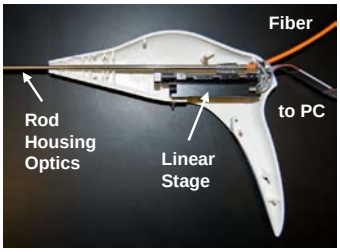

(c)

Fig. 1. Probe design: (a) Optical assembly; (b) Assembled probe; (c) Linear stage

C. Electrical Nerve Stimulation (ENS) Parameters

Identification of the CN was first confirmed by electrical stimulation with simultaneous intracavernous pressure (ICP) measurements. To assess ICP, the shaft of the penis was denuded of skin and the left crural region was cannulated with a 23-G needle connected via polyethylene tubing to a pressure transducer. To electrically stimulate the CN, a bipolar electrode attached to a Grass Instruments S48 stimulator was placed on top of the nerve. Stimulation parameters were 4 V for 30 s at a frequency of 16 Hz with a square wave duration of 5 ms. An increase in ICP after electrical stimulation of the CN was detected by a data acquisition system, and the response parameters were analyzed with MATLAB software.

D. Optical Nerve Stimulation (ONS) Parameters

Optical stimulation of the CN was also performed with simultaneous ICP measurements. ONS of the CN was conducted with a continuous-wave (CW) Thulium fiber laser (TLT-5, IPG Photonics, Oxford, MA) operated at a wavelength of 1870 nm, corresponding to an optical penetration depth of about 400 μm in soft tissue, and chosen to match the rat CN diameter. A function generator was used to modulate the CW laser and produce pulsed output. A 12.7-mm-focal-length calcium fluoride (CaFl) lens was used to focus the beam into the 200-μm fiber. A visible, green aiming beam was coupled into the fiber to provide alignment with the nerve. The fiber tip was kept fixed 2 cm from the CN surface, corresponding to a 1-mm-diameter spot ($1/e^2$), as measured using a razor blade scan. The ONS parameters used were: 3.7 mJ pulse energy, 0.4 J/cm^2 radiant exposure, 5-ms pulse duration, 20 Hz pulse rate, and 1-mm-diameter laser spot, for a 60-s duration. Figure 2 shows the setup used in this study.

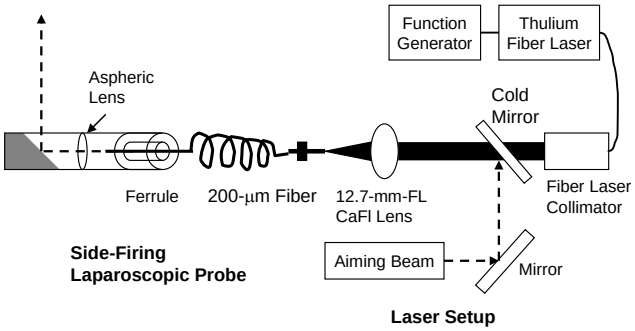

Fig. 2. Diagram of experimental setup with fiber optic assembly for laser probe (left) and laser equipment (right).

E. Animal Surgical Preparation

Four Sprague Dawley rats weighing 400-600 grams were anesthetized by intraperitoneal injection with 50 mg/kg sodium pentobarbital. The rats were secured in the supine position and prepped for surgery. The CN arising from the ipsilateral major pelvic ganglion situated dorsolateral to the prostate was exposed via a midline suprapubic incision and anterior pelvic dissection.

III. RESULTS

A. Fiber Optic Beam Shaping: Computer Simulations

Figure 3 shows the computer simulation results. The laser beam propagates down the fiber with a Gaussian shape and then is transformed to a flat-top profile in free space after traveling beyond the chemically-etched fiber tip. The aspheric collimating lens was placed at a distance of approximately 3.5 mm from the distal fiber tip, to capture this flat-top beam profile.

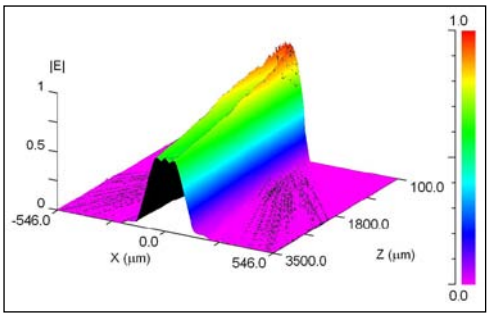

Fig. 3. Computer simulation shows transformation of laser spatial beam profile from Gaussian mode to flat-top mode, after the beam propagates beyond the chemically-etched distal fiber tip.

B. Fiber Optic Beam Shaping: Experimental Results

Figure 4 shows a direct comparison of spatial beam profiles for un-etched distal fiber tip used in Ref. 17, and chemically etched tip used in this study. The un-etched tip approximates a Gaussian beam while the etched tip provides a more uniform flat-top beam profile. This flat-top beam provides more uniform irradiation of the nerve surface and hence safer and more consistent optical nerve stimulation.

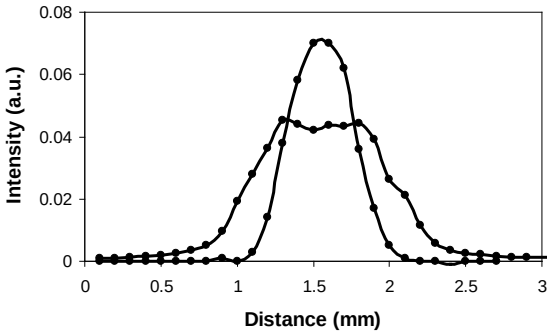

Fig. 4. Comparison of spatial beam profiles after distal fiber tip for unetched (Gaussian) and chemically etched (flat-top) beams.

Razor blade scans were also performed at different working distances from the fiber-lens assembly to measure the laser beam diameter. We were able to achieve the targeted 1 mm ($1/e^2$) spot diameter and obtain collimation of this beam (to within 10% variation) over a distance of about 20 mm, as shown in Figure 5.

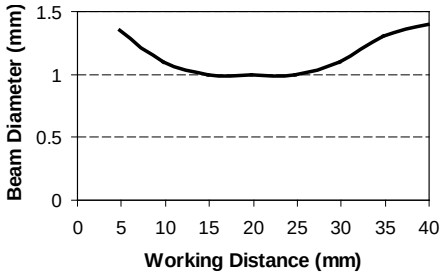

Fig. 5. Beam diameter as a function of working distance (WD). The beam remains at 1 mm diameter (over WD of about 20 mm).

C. Laparoscopic Probe Assembly

Table 1 provides a summary of the optical losses through the experimental laser setup and laparoscopic probe optical components. The transmission rate out of the probe measured approximately 64%. The largest source of losses was the cold mirror used to couple in a green aiming beam into the probe. Due to the relatively uncommon wavelength range of 1850-1880 nm, it was not possible to reduce reflection losses using standard AR coatings.

TABLE I
PROBE TRANSMISSION LOSSES

Optical Component	Losses (%)
Laser System	
Cold Mirror:	- 11.9
Focusing Lens:	- 5.8
Optical Fiber:	- 7.9
Probe	
Aspheric Lens:	- 4.5
Rod Mirror + Tubing:	- 6.0
Transmission (%):	63.9

D. Optical Nerve Stimulation (ONS)

Preliminary testing of the ONS probe was conducted in a rat model, *in vivo*. Figure 6 shows the ICP response of the CN to optical and electrical stimulation for a period of 60 s. ICP increased from a baseline of 17 mmHg to 38 mmHg for ONS. ENS was conducted soon after ONS, with a similar robust ICP response, to demonstrate that the CN did not experience any laser-induced thermal damage. ONS was repeated in four rats with periodic ENS conducted to verify that the laser irradiation parameters were safe.

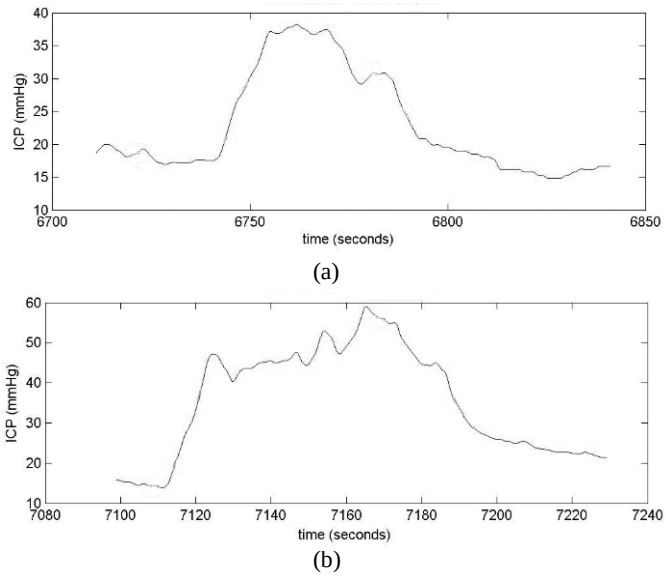

Fig. 6. Comparison of (a) optical and (b) electrical stimulation of the rat cavernous nerves.

IV. DISCUSSION

There is a wide variability in reported sexual potency rates following prostate cancer surgery, due, in part, to the difficulty in preserving the CN during surgery. Any technologies that can assist in identification and preservation of the CN during surgery may lead to direct patient benefit. Optical technologies are ideally suited for use in intra-operative surgical guidance because laser radiation may be delivered through small, flexible optical fibers and easily integrated into surgical instruments for use in laparoscopic and robotic nerve-sparing prostate cancer surgery.

However, a major limitation of optical nerve stimulation is that the window for successfully stimulating the nerve without causing irreversible thermal damage, is relatively narrow. For example, a fluence less than ~ 0.35 J/cm^2 does not produce a reliable response, while a fluence above ~ 0.6-1.0 J/cm^2 may result in increased probability of nerve damage upon long-term, repetitive stimulation [13,14]. Since the fluence at the fiber output end may decrease rapidly due to beam divergence, it is critical that the probe produce a collimated beam over a short working distance (e.g. several millimeters), so that a constant fluence corresponding to safe and reproducible stimulation can be achieved. It may also be important that a flat-top beam profile be used to provide a uniform fluence across the surface of the nerve, to further avoid heat-induced nerve damage during optical stimulation.

The purpose of this study was to design, build, and test a prototype laparoscopic laser nerve stimulation probe, capable of delivering a small, collimated, flat-top spatial beam profile for uniform stimulation of the rat cavernous nerves. Safe and reproducible optical stimulation of the rat cavernous nerve was demonstrated on the first attempt by aiming the laser beam at any region of the exposed nerve.

However, there are several limitations of this study that should be discussed. First, while the rat prostate is the standard small animal model for studies of the cavernous nerves, this model still represents an idealized version of the prostate anatomy. Unlike the human prostate, the rat cavernous nerves are easily visible on the prostate surface. Further testing of our probe will be needed in a larger animal model, such as the canine prostate, which more closely resembles that of the human prostate.

Second, while the beam shaping method applied in this study resulted in a significant improvement in the uniformity of the spatial beam profile, a perfect “tophat” spatial beam profile was not achieved. Further reduction in the wings of the flat-top beam would provide even more uniform irradiation of the nerve surface during optical stimulation. At this time, however, it is unclear if further modifications of the probe optics are warranted, as preliminary rat studies demonstrated safe and reproducible optical nerve stimulation.

Third, while ONS is capable of producing ICP responses similar in magnitude to ENS, the temporal ICP response during ONS varies and may be delayed in comparison with ENS. This slower ICP response during ONS may be dependent on the laser pulse repetition rate. The laser pulse rate may therefore be increased so that sufficient laser energy for stimulation is delivered to the nerve over a shorter time period. However, there is a practical limit to increasing the pulse rate before the onset of thermal damage to the nerve. These conditions need to be explored in more detail.

Finally, during this study, analysis of thermal damage to the nerve after laser nerve stimulation was based on nerve function. Specifically, the ability to achieve a strong ICP response repeatedly with conventional electrical nerve stimulation immediately after laser stimulation was our primary source of feedback. In future studies, once the large matrix of laser nerve stimulation parameters and probe configurations have been fully optimized, histological analysis of the CN will need to be performed, as a more rigorous indicator of thermal damage. Chronic rat studies to determine whether there are any delayed thermal effects to the nerve will also need to be conducted.

V. CONCLUSION

A 3.4-mm-OD laparoscopic probe capable of fitting through a standard 5-mm-ID laparoscopic port, and capable of delivering a collimated, 1-mm-diameter, flat-top laser beam over a working distance of approximately 20 mm was designed, and then successfully tested for optical stimulation of the cavernous nerves in a rat prostate model, *in vivo*. This probe may be useful for noncontact optical stimulation of the cavernous nerves during nerve-sparing laparoscopic prostate cancer surgery.

ACKNOWLEDGMENTS

This research was supported by a grant from the Department of Defense Prostate Cancer Research Program, Grant # PC073709.

REFERENCES

[1] A. L. Burnett, G. Aus, E. D. Canby-Hagino, M. S. Cookson, A. V. D'Amico, R. R. Dmochowski, D. T. Eton, J. D. Forman, S. L. Goldenberg, J. Hernandez, C. S. Higano, S. Kraus, M. Liebert, J. W. Moul, C. Tangen, J. B. Thrasher, I. Thompson, "Erectile function outcome reporting after clinically localized prostate cancer treatment," *J. Urol.*, vol. 178(2), pp. 597-601, 2007.

[2] A. J. Costello, M. Brooks, and O. J. Cole, "Anatomical studies of the neurovascular bundle and cavernosal nerves," *BJU Int.*, vol. 94, pp. 1071-1076, 2004.

[3] L. Klotz, "Neurostimulation during radical prostatectomy: improving nerve-sparing techniques," *Semin. Urol. Oncol.*, vol. 18, pp. 46-50, 2000.

[4] H. L. Kim, D. S. Stoffel, D. A. Mhoon, and C. B. Brendler, "A positive caver map response poorly predicts recovery of potency after radical prostatectomy," *Urol.*, vol. 56, pp. 561-564, 2000.

[5] L. Klotz, J. Heaton, M. Jewett, J. Chin, N. Fleshner, L. Goldenberg, an d M. Gleave, "A randomized phase 3 study of intraoperative cavernous nerve stimulation with penile tumescence monitoring to improve nerve sparing during radical prostatectomy," *J. Urol.*, vol. 164, pp. 1573-1578, 2000.

[6] J. Holzbeierlein, M. Peterson, and J. A. Smith Jr., "Variability of results of cavernous nerve stimulation during radical prostatectomy," *J. Urol.*, vol. 165, pp. 108-110, 2001.

[7] P. C. Walsh, P. Marschke, W. J. Catalona, H. Lepor, S. Martin, R. P. Myers, and M. S. Steiner, "Efficacy of first-generation Cavermap to verify location and function of cavernous nerves during radical prostatectomy: a multi-institutional study by experienced surgeons," *Urol.*, vol. 57, pp. 491-494, 2001.

[8] H. L. Kim, D. A. Mhoon, and C. B. Brendler, "Does the CaverMap device help preserve potency?" *Curr. Urol. Rep.*, vol. 2, pp. 214-217, 2001.

[9] J. Wells, C. Kao, K. Mariappan, J. Albea, E. D. Jansen, P. Konrad, and A. Mahadevan-Jansen, "Optical stimulation of neural tissue in vivo," *Opt. Lett.*, vol. 30, pp. 504-506, 2005.

[10] J. Wells, C. Kao, E. D. Jansen, P. Konrad, and A. Mahadevan-Jansen, "Application of infrared light for in vivo neural stimulation," *J. Biomed. Opt.*, vol. 10:064003, pp. 1-11, 2005.

[11] A. D. Izzo, C. P. Richter, E. D. Jansen, and J. T. Walsh, "Laser stimulation of the auditory nerve," *Lasers Surg. Med.*, vol. 38, pp. 745-753, 2006.

[12] A. D. Izzo, J. T. Walsh, E. D. Jansen, M. Bendett, J. Webb, H. Ralph, and C. P. Richter, "Optical parameter variability in laser nerve stimulation: a study of pulse duration, repetition rate, and wavelength," *IEEE Trans. Biomed. Eng.*, vol. 54, pp. 1108-1114, 2007.

[13] J. D. Wells, S. Thomsen S, P. Whitaker, E. D. Jansen, C. C. Kao, P. E. Konrad, A. Mahadevan-Jansen, "Optical mediated nerve stimulation: identification of injury thresholds," *Lasers Surg. Med.* vol. 39, pp. 513-526, 2007.

[14] N. M. Fried, S. Rais-Bahrami, G. A. Lagoda, A. Y. Chuang, L. M. Su, and A. L. Burnett, "Identification and imaging of the nerves responsible for erectile function in rat prostate, in vivo, using optical nerve stimulation and optical coherence tomography," *IEEE J. Sel. Top. Quant. Electron.*, vol. 13, pp. 1641-1645, 2007.

[15] N. M. Fried, G. A. Lagoda, N. J. Scott, L. M. Su, and A. L. Burnett, "Non-contact stimulation of the cavernous nerves in the rat prostate using a tunable-wavelength thulium fiber laser," *J. Endourol*, vol. 22, pp. 409-413, 2008.

[16] N. M. Fried, G. A. Lagoda, N. J. Scott, L. M. Su, and A. L. Burnett, "Laser stimulation of the cavernous nerves in the rat prostate, in vivo: optimization of wavelength, pulse energy, and pulse repetition rate," *Conf. Proc. IEEE Eng. Med. Biol. Soc.*, vol. 1, pp. 2777-2780, 2008.

[17] S. Tozburun and N. M. Fried, "Design of a compact laparoscopic probe for optical stimulation of the cavernous nerves," *Proc. SPIE*, vol. 716113, pp. 1-4, 2009.

Serhat Tozburun is a Ph.D. student in Optical Science and Engineering at the University of North Carolina at Charlotte.

Mona Mayeh is a Ph.D. student in Optical Science and Engineering at the University of North Carolina at Charlotte.

Gwen A. Lagoda is a research specialist in the Basic Science Laboratory in Neurourology in the Department of Urology at Johns Hopkins Hospital, Baltimore, MD.

Faramarz Farahi is Chairman and Professor of Physics and Optical Science at the University of North Carolina at Charlotte.

Arthur L. Burnett is Professor of Urology at Johns Hopkins Medical School, Baltimore, MD, and Director of the Basic Science Laboratory in Neurourology and the Male Sexual Disfunction Clinic in the Department of Urology at Johns Hopkins Hospital.

Nathaniel M. Fried is an Associate Professor of Physics and Optical Science at the University of North Carolina at Charlotte and an Adjunct Assistant Professor of Urology at Johns Hopkins Medical Institutions. His research interests include therapeutic and diagnostic applications of lasers in urology.

OCT Image Segmentation of the Prostate Nerves

Shahab Chitchian[a], Thomas P. Weldon[b], Nathaniel M. Fried[a,c]

[a] Department of Physics and Optical Science, University of North Carolina at Charlotte, NC
[b] Department of Electrical and Computer Engineering, University of North Carolina at Charlotte, NC
[c] Department of Urology, Johns Hopkins Medical Institutions, Baltimore, MD

ABSTRACT

The cavernous nerves course along the surface of the prostate and are responsible for erectile function. Improvements in identification, imaging, and visualization of the cavernous nerves during prostate cancer surgery may improve nerve preservation and postoperative sexual potency. In this study, 2-D OCT images of the rat prostate were segmented to differentiate the cavernous nerves from the prostate gland. Three image features were employed: Gabor filter, Daubechies wavelet, and Laws filter. The features were segmented using a nearest-neighbor classifier. N-ary morphological post-processing was used to remove small voids. The cavernous nerves were differentiated from the prostate gland with a segmentation error rate of only 0.058 ± 0.019.

1. INTRODUCTION

The cavernous nerves, which are responsible for erectile function, course along the prostate surface and vary in size and location among patients, making identification and preservation of the nerves difficult during removal of a cancerous prostate gland during prostate surgery.[1] Optical coherence tomography (OCT) has recently been tested for imaging of the cavernous nerves in the rat and human prostate.[2–4] However, improvements in identification of the cavernous nerves are necessary prior to clinical use. We recently applied denoising techniques to improve the quality of OCT images.[5,6] In this study, two-dimensional (2D) image segmentation is investigated to differentiate the nerves from the prostate gland.

2. SEGMENTATION SYSTEM

A block diagram of the segmentation system is provided in Fig. 1. The input image $f(x, y)$ is first processed to form three feature images. The features are generated by Gabor filtering, Daubechies wavelet transform, and Laws filter mask, respectively. The prostate image is then segmented into nerve, prostate, and background classes using a k-nearest neighbors classifier and the three feature images. Finally, N-ary morphological post-processing is used to remove small voids.

The first feature image is generated by a Gabor filter.[7] The Gabor feature center frequency of $(0.2, 0.2)$ cycles/pixel, is applied with standard deviations of 3 and 6 in the x and y directions, respectively, based on experimental observation of minimum segmentation error. The second feature is generated by 8-tap Daubechies orthonormal wavelet transform. The third feature is generated by Laws feature extraction method.[8] Laws feature extraction is applied by using the Laws 2 mask. Standard deviation is performed after the Laws mask filtering to complete Laws feature extraction.

The k-nearest neighbors algorithm (k-NN) is a method for classifying objects where classification is based on the k closest training samples in the feature space. A parameter value of $k = 10$ is empirically chosen for the present implementation of the k-nearest neighbors algorithm for segmentation of the prostate images. The prostate image is segmented based on the three feature images forming the feature vector. The Euclidean distance from the image feature vector to all stored vectors are computed, and the k closest samples are selected. A point in the prostate image (cross) is assigned to the nerve class (triangle) if it is the most frequent class label among the k nearest training samples, as shown in Fig. 2. After classification, the N-ary morphological post-processing is applied to remove small voids in the final results.[9]

Further author information: (Send correspondence to Shahab Chitchian)
E-mail: schitchi@uncc.edu, Telephone: 1 704 687 8152, Fax: 1 704 687 8197

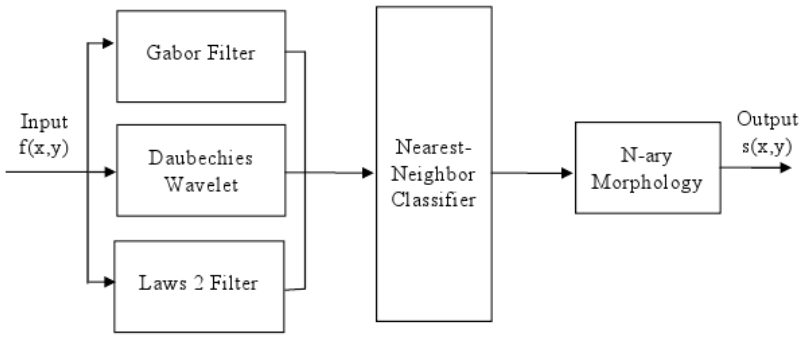

Figure 1. System block diagram. Input image f(x,y) is processed into 3 feature images: Gabor filtered image, 8-tap Daubechies wavelet sub-band, and Laws feature. The features are classified by a k-nearest neighbors classifier into 3 classes: background, nerve, and prostate gland. Finally, an N-ary morphological close and open functions are applied, generating the final output segmented image s(x,y).

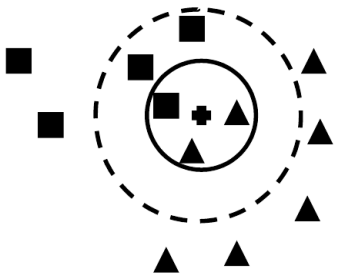

Figure 2. Example of k-nearest neighbors classification. If $k = 3$, a point in the prostate image (cross) is classified to the nerve class (triangle) because there are two triangles and only one square (other class) inside the inner circle. If $k = 5$, a point in the prostate image (cross) is classified to the square class.

3. RESULTS

OCT images were taken *in vivo* in a rat model using a clinical endoscopic OCT system (Imalux, Cleveland, OH) based on an all single-mode fiber (SMF) common-path interferometer-based scanning system (Optiphase, Van Nuys, CA). Mathcad 14.0 (Parametric Technology Corporation, Needham, MA) was used for implementation of the segmentation algorithm described above.

Fig. 3(a,c,e) shows the original OCT images of the cavernous nerves at different orientations (longitudinal, cross-sectional, and oblique) coursing along the surface of the rat prostate. Fig. 3(b,d,f) shows the same OCT images after segmentation using the system of Fig. 1. The cavernous nerves could be differentiated from the prostate gland using this segmentation algorithm.

The overall error rate for the segmentation was 0.058 ± 0.019 which indicates the robustness of our technique. This error rate was obtained by manually creating segmented images and comparing it to the automatic segmentation. Manually segmented images of the cavernous nerves were previously evaluated according to histologic correlation with OCT images.[5]

4. DISCUSSION

Overall, the proposed image segmentation of Fig. 1 performed well for identification of the cavernous nerves in the prostate. Areas that need improvement include the classification of prostate gland in which there are few small scattered regions (shown in white) in the prostate that are erroneously segmented as part of the nerves (e.g. Fig. 3b). To address this limitation a region-based image segmentation method could be used.

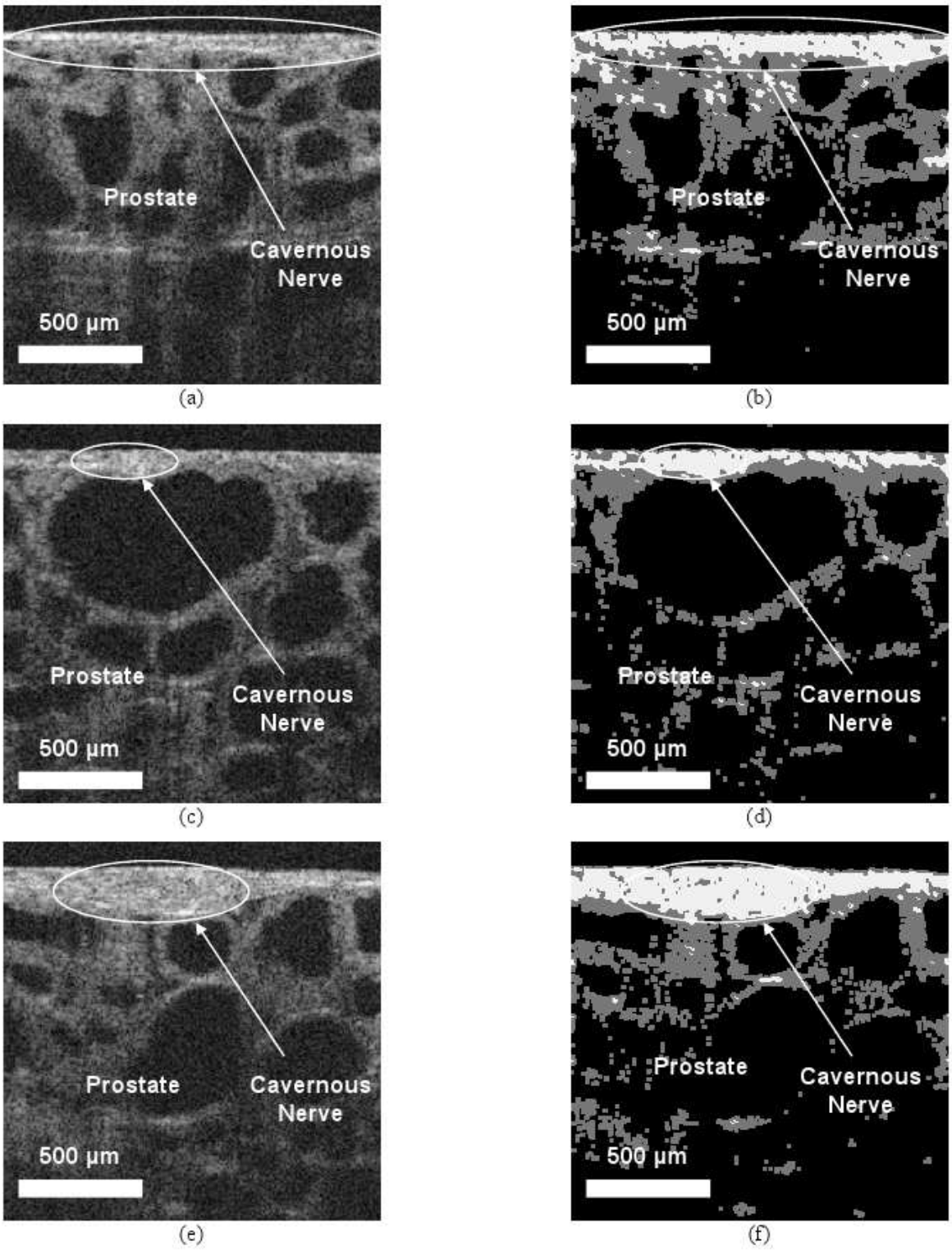

Figure 3. OCT images of the rat cavernous nerve: (a,b) Longitudinal section; (c,d) Cross-section; (e,f) Oblique section. (a,c,e) before; (b,d,f) after segmentation.

It should also be noted that the rat model represents an idealized version of the prostate anatomy because the cavernous nerve lies on the surface of the prostate, and is therefore directly visible. However, in the human anatomy, there may be intervening tissue between the OCT probe and the nerves, making identification more difficult. An important advantage of the proposed classifier-based segmentation approach is that the classifier should also be able to locate the cavernous nerve when it lies at various depths beneath the surface.

5. CONCLUSION

This algorithm for image segmentation of the prostate nerves may prove useful for implementation in clinical endoscopic OCT systems currently being studied for use in laparoscopic and robotic nerve-sparing prostate cancer surgery.

Acknowledgments

This research was supported by the Department of Defense Prostate Cancer Research Program, Grant #PC073709. The authors thank Nancy Tresser of Imalux Corporation (Cleveland, OH) for lending us the Niris OCT system for these studies.

REFERENCES

[1] Murphy, G., Mettlin, C., Menck, H., Winchester, D., and Davidson, A., "National patterns of prostate cancer treatment by radical prostatectomy: results of a survey by the american college of surgeons committee," *Cancer. J. Urol.* **152**, 1817–1819 (1994).

[2] Aron, M., Kaouk, J., Hegarty, N., Colombo, J., Haber, G., Chung, B., Zhou, M., and Gill, I., "Preliminary experience with the niris optical coherence tomography system during laparoscopic and robotic prostatectomy," *J. Endourol.* **21**(8), 814–818 (2007).

[3] Fried, N., Rais-Bahrami, S., Lagoda, G., Chuang, A., Burnett, A., and Su, L., "Imaging the cavernous nerves in rat prostate using optical coherence tomography," *Lasers Surg. Med.* **39**(1), 36–41 (2007).

[4] Rais-Bahrami, S., Levinson, A., Fried, N., Lagoda, G., Hristov, A., Chuang, A., Burnett, A., and Su, L., "Optical coherence tomography of cavernous nerves: A step toward real-time intraoperative imaging during nerve-sparing radical prostatectomy," *Urology* **72**, 198–204 (2008).

[5] Chitchian, S., Fiddy, M., and Fried, N., "Optical coherence tomography of the prostate nerves via wavelet shrinkage using dual-tree complex wavelet transform," *J. Biomed. Opt.* **14**, 014031 (2009).

[6] Chitchian, S., Fiddy, M., and Fried, N., "Speckle reduction during all-fiber common-path optical coherence tomography of the cavernous nerves," *Proc. SPIE* **7168**, 71682N (2009).

[7] Weldon, T., Higgins, W., and Dunn, D., "Efficient gabor filter design for texture segmentation," *Pattern Recognition* **29**, 2005–2015 (1996).

[8] Pratt, W., [*Digital Image Processing*], Wiley (2007).

[9] Weldon, T., "Removal of image segmentation boundary errors using an n-ary morphological operator," *Proc. of IEEE Southeast Conf.* , 509–513 (2007).

Near-IR Optical Properties of Canine Prostate Tissue using Oblique-Incidence Reflectometry

Shahab Chitchian[a] and Nathaniel M. Fried*[a,b]

[a] Department of Physics and Optical Science, University of North Carolina at Charlotte, NC
[b] Department of Urology, Johns Hopkins Medical Institutions, Baltimore, MD

ABSTRACT

Optical imaging systems utilizing near-infrared light sources such as optical coherence tomography (OCT) have recently been used for imaging the prostate gland. However, the optimal wavelength for deep imaging of the prostate has yet to be determined. The objective of this study is to determine the optimal near-infrared wavelength for OCT imaging of the prostate using a system that has the potential to be used in an in vivo model. An oblique-incidence single point measurement technique using a normal-detector scanning system was implemented to determine the absorption (μ_a) and reduced scattering coefficients (μ'_s) of fresh canine prostate tissue, *ex vivo*, from the diffuse reflectance profile of near-IR light as a function of source-detector distance. The effective attenuation coefficient (μ_{eff}) and optical penetration depth (OPD) were then calculated for near-IR wavelengths of 1064, 1307, and 1555 nm. A total of ten canine samples were used for this study. At wavelengths of 1064, 1307, and 1555 nm, the mean absorption coefficients measured 0.08 $\pm$ 0.03, 0.12 $\pm$ 0.04, and 0.23 $\pm$ 0.09 cm^{-1}, respectively. The mean reduced scattering coefficients measured 16.60 $\pm$ 0.95, 14.30 $\pm$ 1.14, and 10.98 $\pm$ 2.35 cm^{-1}. The effective attenuation coefficients were calculated to be 2.00, 2.28, and 2.78 cm^{-1}, yielding OPD's of 0.5, 0.44, and 0.36 cm at 1064, 1307, and 1555 nm. OCT imaging studies of the prostate may benefit from replacement of commonly used 1310 nm broadband light sources with 1064 nm sources.

Key Words: optical properties, diffuse reflectance spectroscopy, prostate, optical coherence tomography, OCT

1. INTRODUCTION

Near-infrared wavelength light sources are commonly used in optical coherence tomography (OCT) of the prostate gland [1-5]. While the optical properties of prostate tissue at visible (600 nm's) and near-visible (700 nm's) wavelengths are well characterized due to interest in photodynamic therapy for prostate cancer [6-9], the optimal wavelength for deep penetration of near-IR light into prostate tissue for OCT of the prostate gland has yet to be determined. Knowledge of the optical properties of prostate tissue at these near-IR wavelengths would provide critical data for optimization of OCT systems. The optical properties of interest are the absorption coefficient, μ_a, and the scattering coefficient, μ_s. The reduced scattering coefficient, μ'_s, is composed of the product $\mu_s(1\text{-}g)$, where g is the anisotropy factor defined as the average cosine of the scattering angle. An increase in either μ_a or μ'_s increases the attenuation of light, thus decreasing penetration depth.

The most common technique for measuring optical properties of biological tissues is the double integrating-sphere technique. However, this technique is invasive and requires the removal of a thin slice of tissue [10]. Time-resolved spectroscopy has also been used but requires expensive laser instrumentation [9]. Another technique is normal-incidence or oblique-incidence reflectometry [11,12]. This technique, which is based on diffusion theory, provides a simple, inexpensive, and noninvasive method to determine tissue optical properties. Marquez et al. [11] utilized oblique-incidence fiber-optic reflectometry and Joshi et al. [12] applied normal-incidence reflectometry using a steady-state imaging technique. In this paper, an oblique-incidence single point measurement technique with a normal-detector scanning system is designed to resolve the spatial distribution of diffuse reflectance. Then, using a Levenberg-Marquardt algorithm, the absorption and reduced scattering coefficients are calculated by fitting the measurement to the modified dipole source diffusion-theory model.

*nmfried@uncc.edu; phone: 1 704 687 8149; fax: 1 704 687 8197

The objective of this study is to determine the optimal near-IR wavelength for OCT imaging of the prostate gland using a system that has the potential to be used in an in vivo animal and human model in the near future. We determine the optical properties μ_a, μ'_s, and μ_{eff} of canine prostate tissue at wavelengths of 1064 nm, 1307 nm, and 1555 nm, in which broadband light sources for OCT imaging are commonly available.

2. MATERIALS AND METHODS

When light enters a semi-infinite tissue, it will generally scatter a multiple times before either being absorbed or exiting the tissue surface at a point other than its point of entry. Diffuse reflectance is the multiply scattered light which escapes the tissue surface. Resolving the optical properties of tissue from diffuse reflectance is a simple approach. We utilize a simple two-source diffusion theory model of spatially resolved, steady-state diffuse reflectance for this purpose [13]. It is easier to model isotropic scattering than anisotropic scattering, so the reduced scattering coefficient μ'_s is introduced as,

$$\mu_s' = \mu_s\left(1-g\right) \tag{1}$$

where μ_s is the scattering coefficient and g is the average cosine of the scattering angle.

The modified dipole source diffusion-theory model gives diffuse reflectance as [11]

$$R\left(x\right) = \frac{\Delta z\left(1+\mu_{eff}\,\rho_1\right)\exp\left(-\mu_{eff}\,\rho_1\right)}{4\pi\rho_1^3} + \frac{\left(\Delta z + 2z_b\right)\left(1+\mu_{eff}\,\rho_2\right)\exp\left(-\mu_{eff}\,\rho_2\right)}{4\pi\rho_2^3} \tag{2}$$

where x is the distance to the point of illumination; $\rho_1 = \sqrt{x^2+\Delta z^2}$ and $\rho_2 = \sqrt{x^2+\left(\Delta z + 2z_b\right)^2}$ are the distances to the dipole sources; $\Delta z = \frac{\cos\alpha_t}{0.35\mu_a + \mu_s'}$ is the depth of the positive point source; $z_b = 2AD$ is the distance between the virtual boundary and the surface of the tissue; α_t is the angle of refraction; $\mu_{eff} = \sqrt{\frac{\mu_a}{D}}$ is the effective attenuation coefficient; $D = \frac{1}{3\left(0.35\mu_a + \mu_s'\right)}$ is the diffusion coefficient for media with scattering dominating absorption; $A = \frac{1+r_i}{1-r_i}$ is unity for a matched boundary; and $r_i = -1.440n_{rel}^{-2} + 0.710n_{rel}^{-1} + 0.668 + 0.0636n_{rel}$ is the internal diffuse reflectance, where $n_{rel} = \frac{n_{tissue}}{n_{ambient}} = 1.4$ [14].

Our experimental setup, shown in Figure 1, consists of a sample holder for the prostate tissue, an InGaAs detector (PDA400, Thorlabs, Newton, NJ) aligned normal to the tissue surface, a 25.4-mm-focal-length plano-convex lens (Thorlabs) mounted in a lens tube for collecting the light from a 0.1 mm point of the tissue surface in each scan, a digital oscilloscope (TDS 2002B, Tektronix, Beaverton, OR) to record the measured data by detector, linear actuators (850G, Newport, Irvine, CA) for scanning the detector along the tissue surface, a motion controller (ESP300, Newport) for controlling the linear actuators, 1064 nm, 1307 nm, and 1555 nm laser diodes (QFLD, Qphotonics, Ann Arbor, MI), a laser diode controller (6000, Newport) for operating the laser diodes and a 35.0-mm plano-convex lens (Thorlabs) to illuminate a single point on the tissue surface. The experiment was automated using LabVIEW software (National Instruments, Austin, TX). The prostate surface was sufficiently large to assume the sample to be semi-infinite with no light reflected at the boundaries.

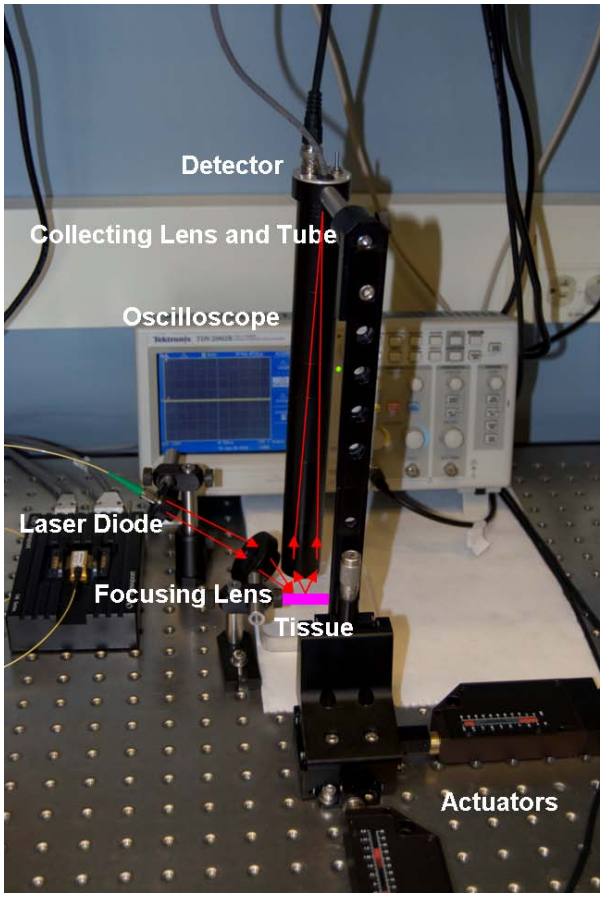

Figure 1. Experimental setup. The prostate tissue is illuminated with a narrow beam of light at an incident angle on its surface and the radiant emittance is measured as a function of distance to the point of illumination.

Our measurement method consisted of the following two steps:

1. The prostate sample was illuminated with a focused beam of light, 0.5 mm ($1/e^2$) diameter, at each wavelength with the incident angle of $\alpha_i=60^\circ$ onto its surface and the radiant emittance was measured as a function of distance to the point of illumination. The focal area of the detector which collects the light was 1 mm diameter. The setup was designed to collect reflective light from an area of 0.1 mm diameter. The detector was scanned on a 10 mm line across the tissue surface at a normal angle with a resolution of 0.1 mm. Therefore, 100 points were collected and the last 90 points were used for fitting the raw data and the theory, because the diffusion theory does not accurately model near diffuse reflectance [11]. The radiant emittance was divided by a calibrated scale factor of the light source intensity to obtain diffuse reflectance.

2. The absorption and reduced scattering coefficients were calculated by fitting the measurement to the diffuse reflectance, Eq. 2, using the Levenberg-Marquardt algorithm. Figure 2 shows an example of fitting between the measurement and the theory in one scan sample. The effective attenuation coefficient and Optical Penetration Depth (OPD) were calculated by $\mu_{eff} = \sqrt{3\mu_a\left(\mu_a + \mu_s'\right)}$ and $OPD = \dfrac{1}{\mu_{eff}}$, respectively.

The canine prostate was chosen for these preliminary studies because it represents the best large animal model for simulating the human prostate gland, and has been commonly used in previous optical property studies [6,7,14]. Canine prostate glands were harvested from dogs sacrificed for unrelated experiments. The samples were then stored in saline in a refrigerator and used within 24 hours of collection. Prior to use, the prostate samples were sectioned into dimensions of 4 × 3 cm with a thickness of 1.5 cm. The sectioned tissue samples were kept hydrated with saline to mimic the normal water content of prostate tissue, *in vivo*. The optical properties, μ_a and μ'_s, of 10 fresh canine prostate tissue samples were measured, *ex vivo*, at 1064 nm, 1307 nm, and 1555 nm.

3. RESULTS

Results of the optical property measurements are presented in Table 1. The mean values of coefficients for these samples were calculated to determine the effective attenuation coefficient, μ_{eff}, and OPD. Since Oraevsky and Jacques (Appendix, Ch. 8) [10] and Nau *et al.* [14] previously reported the optical properties of canine prostate tissue at 1064 nm, we used their results as a reference to validate our method. Their coefficients were reported as μ_a=0.04 and 0.27 cm^{-1}, and μ'_s=13 and 17.6 cm^{-1}, respectively, compared to our measurements of μ_a=0.08 cm^{-1}, and μ'_s=16.6 cm^{-1}. Thus, for the 1064 nm wavelength, our results fall within the range of previously reported values.

Table 1. Summary of canine prostate optical properties.

Coefficients (cm^{-1})	Sample No.	1064 nm	1307 nm	1555 nm
μ'_s	1	16.24	14.54	11.59
	2	16.50	14.51	9.84
	3	17.25	16.58	13.87
	4	18.10	15.57	14.44
	5	15.28	14.02	9.86
	6	17.62	14.21	12.52
	7	17.16	13.07	9.25
	8	15.86	14.38	8.55
	9	15.31	13.05	7.37
	10	16.66	13.05	12.50
	Mean	**16.60**	**14.30**	**10.98**
	σ	**0.95**	**1.14**	**2.35**
μ_a	1	0.11	0.10	0.18
	2	0.08	0.13	0.20
	3	0.06	0.07	0.20
	4	0.07	0.07	0.10
	5	0.12	0.11	0.23
	6	0.04	0.12	0.15
	7	0.03	0.22	0.24
	8	0.12	0.13	0.40
	9	0.12	0.13	0.27
	10	0.08	0.15	0.33
	Mean	**0.08**	**0.12**	**0.23**
	σ	**0.03**	**0.04**	**0.09**
μ_{eff}	**Mean**	**2.00**	**2.28**	**2.78**
OPD	**Mean**	**0.50**	**0.44**	**0.36**

The values of μ_a and μ'_s showed significant differences between 1064 nm, 1307 nm, and 1555 nm. A paired t-test was performed for comparison of different wavelengths, with statistical significance given by values of $P < 0.05$. Comparison of 1064 nm to 1307 nm resulted in P values of 0.0001 and 0.0325 for μ'_s and μ_a, respectively. Comparison of 1307 nm to 1555 nm yielded P values of 0.0008 and 0.0026 for μ'_s and μ_a, respectively. All of these values are considered to be statistically significant.

4. DISCUSSION

The results of this study suggest that future OCT prostate imaging studies may benefit from replacement of commonly used 1310 nm broadband light sources with 1064 nm sources. The reduced scattering coefficient, μ'_s, decreased with increasing wavelengths, predominantly because of the strong wavelength dependence of Rayleigh scattering. Conversely, the absorption coefficient increased at longer wavelengths due to increased water absorption. At longer wavelengths, increased water absorption outweighed decreased scattering in the tissue and resulted in a reduced optical penetration depth.

We also compared the optical penetration depth for *ex vivo* canine prostate at 633 nm and 1064 nm according to the optical property coefficients reported by Nau *et al.* [14]. The OPDs were calculated as 0.14 cm and 0.26 cm at 633 nm and 1064 nm, respectively, demonstrating that 1064 nm has greater penetration depth than shorter visible wavelengths, such as 633 nm.

However, it should be noted that Zhu *et al.* reported significantly greater penetration depths for canine and human prostate at 732 nm [7,8]. Although we did not perform experiments at 732 nm, the trends in our results at longer near-infrared wavelengths, combined with those results reported by Nau *et al.* [14] at 633 nm do not support the penetration depths reported by Zhu *et al.* [7]. Future studies may need to address these differences in more detail.

Finally, it should be noted that there are some errors in the fitting process used for the diffusion model, shown in Figure 2. However, in comparison to the steady-state imaging technique [12], the robustness and reliability of our technique appears to be an improvement.

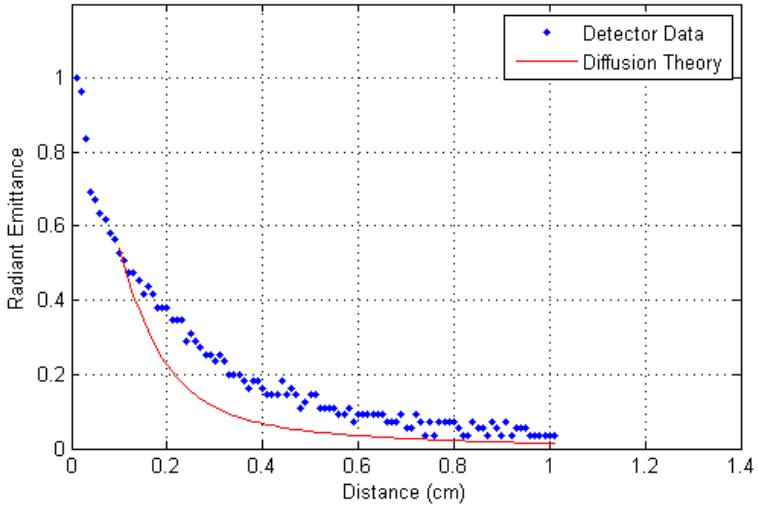

Figure 2. The absorption and reduced scattering coefficients are calculated by fitting the measurement to the diffuse reflectance.

5. CONCLUSIONS

The optical properties μ_a, μ'_s, μ_{eff}, and OPD of ex vivo canine prostate tissue at wavelengths of 1064 nm, 1307 nm, and 1555 nm were determined by utilizing a simple two-source diffusion theory model of spatially resolved, steady-state diffuse reflectance. Knowledge of these optical properties is essential for the development of optimized optical coherence tomography systems for deep imaging of the prostate. The results of this study suggest that OCT prostate imaging studies may benefit from replacement of commonly used 1310 nm broadband light sources with 1064 nm sources. Future studies will focus on miniaturization of the experimental setup for potential use in *in vivo* studies, and decreasing uncertainties and errors in the measurement process for the technique.

6. ACKNOWLEDGMENTS

This research was supported by the Department of Defense Prostate Cancer Research Program, Grant #PC073709. The authors wish to thank Christina Crothers for her assistance in harvesting tissue for the experiments.

REFERENCES

[1] D'Amico, A., Weinstein, M., Li, X., Richie, J., and Fujimoto, J., "Optical coherence tomography as a method for identifying benign and malignant microscopic structures in the prostate gland," Urology 55, 783-787 (2000).

[2] Aron, M., Kaouk, J., Hegarty, N., Colombo, J., Haber, G., Chung, B., Zhou, M., and Gill, I., "Preliminary experience with the niris optical coherence tomography system during laparoscopic and robotic prostatectomy," J. Endourol. 21, 814-818 (2007).

[3] Fried, N., Rais-Bahrami, S., Lagoda, G., Chuang, A., Burnett, A., and Su L, "Imaging the cavernous nerves in rat prostate using optical coherence tomography," Lasers Surg. Med. 39, 36-41 (2007).

[4] Chitchian, S., Fiddy, M., and Fried, N, "Denoising during optical coherence tomography of the prostate nerves via wavelet shrinkage using dual-tree complex wavelet transform," J. Biomed. Opt. 14:014031 (2009).

[5] Chitchian, S., Weldon, T., and Fried, N, "Segmentation of optical coherence tomography images for differentiation of the cavernous nerves from the prostate gland," J. Biomed. Opt. 14:044033 (2009).

[6] Chen, Q., Wilson, B., Shetty, S., Patterson, M., Cerny, J., Hetzel, F., "Changes in in vivo optical properties and light distributions in normal canine prostate during photodynamic therapy," Radiat. Res. 147, 86-91 (1997).

[7] Zhu, T., Hahn, S., Kapatkin, A., Dimofte, A., Rodriquez, C., Vulcan, T., Glatstein, E., and His, R., "In vivo optical properties of normal canine prostate at 732 nm using motexafin lutetium-mediated photodynamic therapy," Photochem. Photobiol. 77, 81-88 (2003).

[8] Zhu, T., Dimofte, A., Finlay, J., Stripp, D., Busch, T., Miles, J., Whittington, R., Malkowicz, B., Tochner, Z., Glatstein, E., and Hahn, S, "Optical properties of human prostate at 732 nm measured in vivo during motexafin lutetium-mediated photodynamic therapy," Photochem. Photobiol. 81, 96-105 (2005).

[9] Svensson, T., Andersson-Engels, S., Einarsdottir, M., and Svanberg, K., "In vivo optical characterization of human prostate tissue using near-infrared time-resolved spectroscopy," J. Biomed. Opt. 12:014022 (2007).

[10] Wilson B., "Measurement of tissue optical properties: methods and theories," In: Welch A, van Gemert M, eds. Optical-thermal response of laser-irradiated tissue. New York: Plenum Press, 233-303 (1995).

[11] Marquez, G., Wang, L., Lin, S., Schwartz, J., and Thomsen, S., "Anisotropy in the absorption and scattering spectra of chicken breast tissue," Appl. Opt. 37, 798-804 (1998).

[12] Joshi, N., Donner, C., and Jensen, H., "Noninvasive measurement of scattering anisotropy in turbid materials by nonnormal incident illumination," Opt. Letters 31, 936-938 (2006).

[13] Farrell, T. and Patterson, M., "A diffusion theory model of spatially resolved, steady-state diffuse reflectance for the noninvasive determination of tissue optical properties in vivo," Med. Phys. 19, 879-888 (1992).

[14] Nau, W., Roselli, R., and Milam, D., "Measurement of thermal effects on the optical properties of prostate tissue at wavelengths of 1,064 and 633 nm," Lasers Surg. Med. 24, 38-47 (1999).

Incorporation of Fiber Optic Beam Shaping into a Laparoscopic Probe for Laser Stimulation of the Cavernous Nerves

Serhat Tozburun[a], Gwen A. Lagoda[b], Mona Mayeh[a],
Arthur L. Burnett[b], Faramarz Farahi[a], and Nathaniel M. Fried[ab*]

[a] Department of Physics and Optical Science, University of North Carolina at Charlotte, NC
[b] Department of Urology, Johns Hopkins Medical Institutions, Baltimore, MD

ABSTRACT

The cavernous nerves (CN) course along the prostate surface and are responsible for erectile function. Improved identification and preservation of the CN's is critical to maintaining sexual potency after prostate cancer surgery. Noncontact optical nerve stimulation (ONS) of the CN's was recently demonstrated in a rat model, *in vivo*, as a potential alternative to electrical nerve stimulation (ENS) for identification of the CN's during prostate surgery. However, the therapeutic window for ONS is narrow, so optimal design of the fiber optic delivery system is critical for safe, reproducible stimulation. This study describes modeling, assembly, and testing of an ONS probe for delivering a small, collimated, flat-top laser beam for uniform CN stimulation. A direct comparison of the magnitude and response time of the intracavernosal pressure (ICP) for both Gaussian and flat-top spatial beam profiles was performed. Thulium fiber laser radiation (λ=1870 nm) was delivered through a 200-μm fiber, with distal fiber tip chemically etched to convert a Gaussian to flat-top beam profile. The laser beam was collimated to a 1-mm-diameter spot using an aspheric lens. Computer simulations of light propagation were used to optimize the probe design. The 10-Fr (3.4-mm-OD) laparoscopic probe provided a constant radiant exposure at the nerve surface. The probe was tested in four rats, *in vivo*. ONS of the CN's was performed with a 1-mm-diameter spot, 5-ms pulse duration, and pulse rate of 20 Hz for a duration of 15-30 s. The flat-top laser beam profile consistently produced a faster and higher ICP response at a lower radiant exposure than the Gaussian beam profile due, in part, to easier alignment of the more uniform beam with nerve. With further development, ONS may be used as a diagnostic tool for identification of the CN's during laparoscopic and robotic nerve-sparing prostate cancer surgery.

Key Words: optical stimulation, nerve, prostate, cavernous nerves, neurovascular bundle

1. INTRODUCTION

The cavernous nerves (CN) are responsible for erectile function. Variation in size and anatomic location of the CN's among patients makes nerve preservation difficult during prostate cancer surgery. As a result, there is wide variability in sexual function rates (9-86%) following prostate surgery [1]. Any technology capable of improved identification and preservation of the CN's would result in improved sexual function and direct patient benefit.

Recently, optical nerve stimulation (ONS) has been demonstrated using pulsed infrared lasers [2]. ONS offers several advantages over electrical nerve stimulation (ENS), including: (1) a non-contact method of stimulation, (2) improved spatial selectivity, and (3) elimination of stimulation artifacts.

We have recently demonstrated successful ONS of the CN's in a rat model, *in vivo* [3]. This technique may have the potential to be used as an alternative method to ENS as a diagnostic tool for identifying and preserving the CN's during prostate surgery. However, a major limitation of ONS is that a narrow range of radiant exposures is necessary for safe, reproducible nerve stimulation. Radiant exposures less than ~ 0.35 J/cm^2 may not produce a reliable and a consistent ICP response, while higher radiant exposures of ~ 0.6-1.0 J/cm^2 may result in nerve damage with repetitive stimulation [3,4]. The laser beam diverges rapidly after exiting the fiber, making the beam diameter highly dependent on working distance. Therefore, it is critical that an ONS probe produce a collimated beam over a short working distance to provide a constant radiant exposure corresponding to safe, reproducible nerve stimulation.

*nmfried@uncc.edu; phone: 1 704 687 8149; fax: 1 704 687 8197

Preliminary work in our laboratory reported the design of an ONS probe with a collimated beam [5], and included fiber optic beam shaping methods for converting the Gaussian to flat-top beam profile with preliminary testing of the probe in a rat cavernous nerve model, *in vivo* [6].

The objective of this study is to directly compare the magnitude and response time of ICP as a function of radiant exposure for the Gaussian and flat-top spatial beam profile in a rat cavernous nerve model, *in vivo*. An ONS probe design capable of producing a fast and strong ICP response at a low radiant exposure would make the use of ONS more attractive as a diagnostic tool during laparoscopic and robotic nerve-sparing prostate cancer surgery.

2. MATERIALS AND METHODS

A 200-μm-core, low-OH silica optical fiber (BFL22-200, Thorlabs, Newton, NJ) with a 0.22 NA was used in these studies. The core of the distal fiber tip was etched with hydrofluoric (HF) acid for 1 min at room temperature and then cleaned with distilled (DI) water. During the acid etching process, the fiber was surrounded by 49% HF acid diluted with DI water in a 1:4 ratio (acid/water). The central 100 μm of the fiber tip was chemically etched to a depth of approximately 2 μm.

Computer simulations using fiber optic ray tracing software (RSoft Photonics CAD Suite Version 8.0.1.), based on advanced finite difference beam propagation techniques, were used to help optimize the chemical etching conditions necessary to provide a flat-top spatial beam profile.

A 5.5-Watt Thulium fiber laser (TLT-5, IPG Photonics, Inc, Oxford, MA) with tunable wavelength range of 1850-1880 nm was used for ONS in these studies. An aspheric lens (2-mm-OD, 350430-C, Thorlabs) and glass ferrule (Vitrocom, Mountain Lakes, NJ) were glued into place inside a quartz capillary tube (2.0-mm-ID, 2.4-mm-OD, CV2024, Vitrocom). Either an un-etched or etched 200-μm-core low-OH silica optical fiber (BFL22-200, Thorlabs) with 0.22 NA were inserted into a glass ferrule (Vitrocom) for centering with the optics, and then glued into place inside the glass capillary tubing. A green aiming beam for alignment and the infrared laser beam were coupled into a 200-μm-core-diameter fiber by using a 12.7-mm-focal-length calcium fluoride lens. Figure 1 provides a diagram of the experimental setup and details of the optical components.

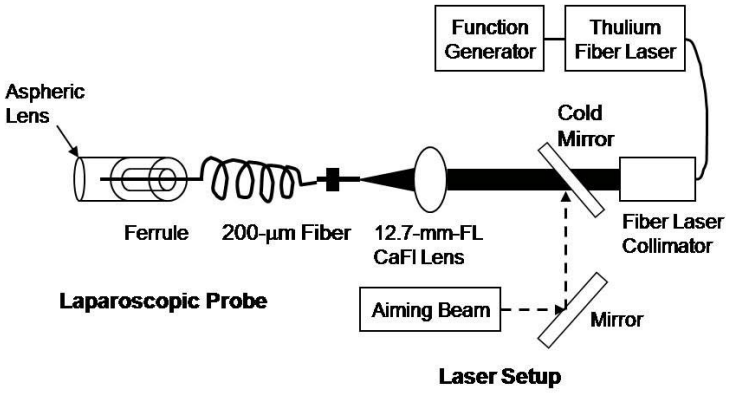

Figure 1. Diagram of experimental setup with fiber optic assembly for probe (left) and laser (right).

3. RESULTS

Figure 2 shows the computer simulation results in both 2D and 3D formats. The laser beam propagates down the fiber with a Gaussian shape and then the beam is transformed to a flat-top profile in free space after traveling through the chemically-etched fiber tip. The aspheric collimating lens is placed at a distance of approximately 3.5 mm from the distal fiber tip, to capture and collimate this flat-top beam profile.

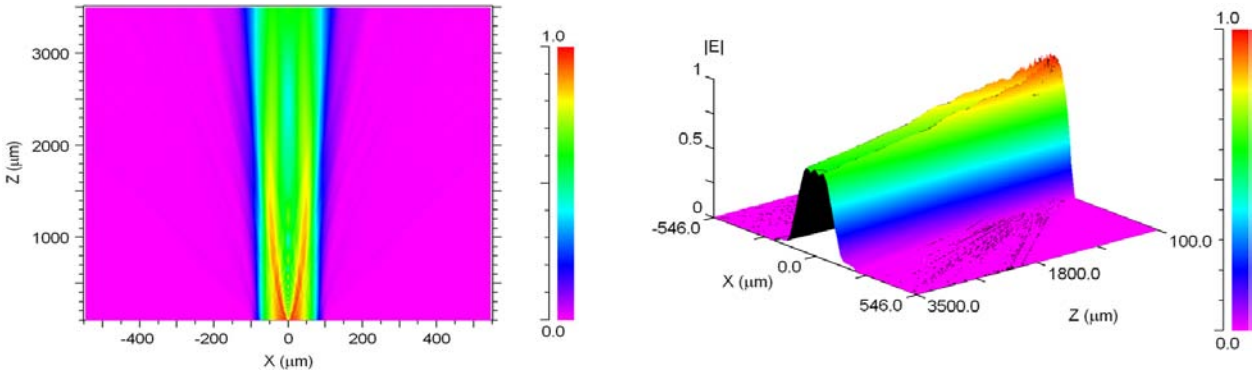

(a) (b)

Figure 2. Computer simulation shows transformation of laser spatial beam profile from Gaussian mode to flat-top mode in (a) 2D cross-section and (b) 3D after the beam propagates through the chemically-etched distal fiber tip.

The beam diameter was measured by performing razor blade scans at different distances from the output end of the probe. An approximately 1 mm ($1/e^2$) spot diameter and collimated beam was obtained over a working distance of 15-30 mm for both the (a) Gaussian (b) and flat-top probes (Figure 3).

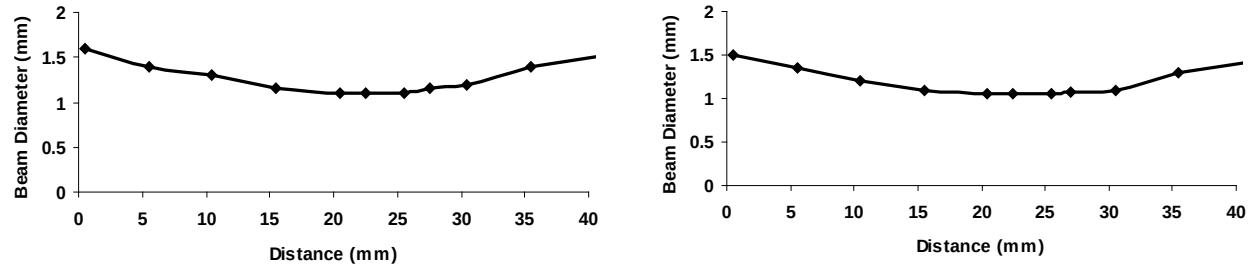

(a) (b)

Figure 3. Beam diameter of Gaussian (a) and Flat-top (b) probes as a function of working distance. The spot diameters remain at approximately 1 mm diameter over a working distance of 15-30 mm.

A direct comparison of the beam profiles for the un-etched and chemically etched fibers is shown in Figure 4. The un-etched fiber tip produces a Gaussian beam profile and the etched tip provides a relatively more uniform intensity distribution on the nerve surface as a flat-top spatial beam profile.

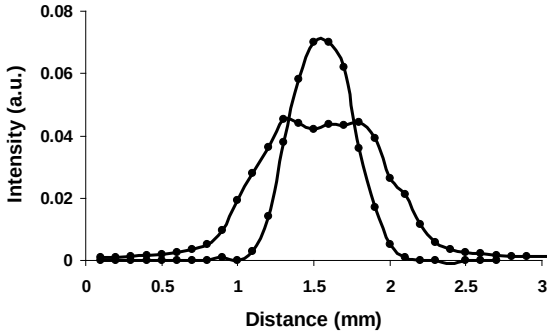

Figure 4. Comparison of spatial beam profiles at the distal fiber tip of un-etched and chemically etched fibers.

The spatial beam profiles at the output end of the (a,b) Gaussian and (c,d) flat-top probes are shown in Figure 5. The 2D and 3D images were acquired with an infrared beam analyzer (Pyrocam III, Spiricon, Logan UT).

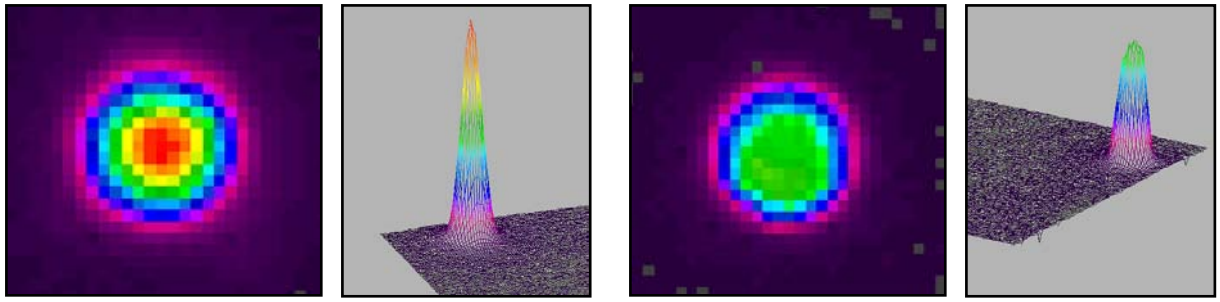

(a) (b) (c) (d)

Figure 5. Spatial beam profiles taken with an infrared beam analyzer: (a,b) Gaussian and (c,d) Flat-top spatial beam profiles.

Plots of the ICP response for the cavernous nerve for both Gaussian (a) and flat-top (b) spatial beam profiles as a function of radiant exposure are shown in Figure 6. The ONS parameters used in Figure 6a were 5-ms pulse duration, 20 Hz, and 1-mm-diameter laser spot, for a 30 s duration. In Figure 6b, the OSN parameters used were 5-ms pulse duration, 20 Hz, and about 1-mm-diameter laser spot, for a 15 s duration. The longer stimulation time in Figure 6a was necessary due to the weaker and slower ICP response time of the Gaussian beam profile. Faster and higher ICP responses of the CN were obtained at a lower radiant exposure for the flat-top versus the Gaussian beam profile. This may be due, in part, to improved alignment of a flat-top beam with the nerve by providing a more uniform intensity distribution across the nerve surface.

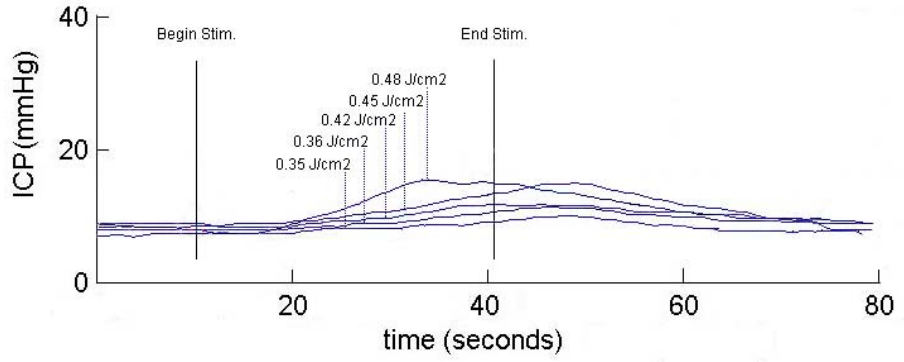

(a)

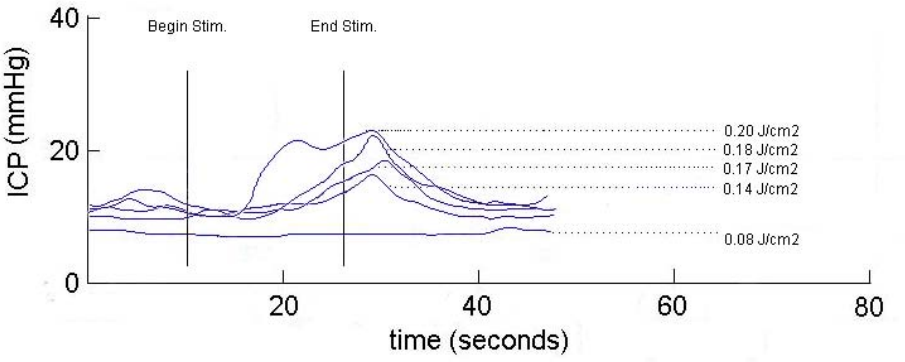

(b)

Figure 6. Comparison of (a) Gaussian and (b) flat-top spatial beam profiles for optical stimulation of the rat cavernous nerves as a function of radiant exposure. The magnitude of the ICP increases and the response time decreases as the radiant exposure is increased for both beam profiles. However, by comparison, the ICP response is significantly higher and faster for the flat-top beam profile at lower radiant exposures than for the Gaussian beam profile.

4. DISCUSSION

There is a wide variability in reported sexual potency rates following prostate cancer surgery, due, in part, to the difficulty in preserving the CN during surgery. Any technologies that can assist in identification and preservation of the CN during surgery may lead to direct patient benefit.

This study compares probes producing Gaussian and flat-top spatial beam profiles for ONS of the CN's in a rat model, *in vivo*. Both laparoscopic probes delivered a 1-mm-diameter, collimated beam at a working distance of about 20 mm from the CN. For the same laser parameters (pulse duration = 5 ms, pulse rate = 20 Hz), the flat-top beam profile produced a faster and higher ICP response at a lower radiant exposure than the Gaussian beam profile.

There are several limitations of this study that should be discussed. First, while the rat prostate is the standard small animal model for cavernous nerve studies, this model represents an idealized version of the prostate anatomy. Unlike the human prostate, the rat cavernous nerves are easily visible on the prostate surface. Further testing of our probe will be needed in a larger, canine prostate model which more closely resembles the human prostate.

Second, while the beam shaping method applied in this study resulted in a significant improvement in the uniformity of the spatial beam profile, a perfect "tophat" spatial beam profile was not achieved. Further reduction in the wings of the flat-top beam would provide even more uniform irradiation of the nerve surface during optical stimulation.

Finally, analysis of thermal damage to the nerve after laser nerve stimulation was based on nerve function in this study. Specifically, the ability to achieve a strong ICP response repeatedly with conventional electrical nerve stimulation immediately after laser stimulation was our primary source of feedback. In future studies, once the large matrix of laser nerve stimulation parameters and probe configurations have been fully optimized, histological analysis of the CN will need to be performed, as a more rigorous indicator of thermal damage. Chronic rat studies to determine whether there are any delayed thermal effects to the nerve will also need to be conducted.

5. CONCLUSIONS

A 3-mm-OD laparoscopic probe capable of delivering a collimated, 1-mm-diameter, flat-top laser beam was designed and successfully tested for optical nerve stimulation. This probe produced a faster and higher ICP response in the rat CN at a lower radiant exposure than for a standard probe with a Gaussian beam profile. With further development, this probe may be useful for safe and reproducible noncontact optical stimulation of the cavernous nerves during nerve-sparing laparoscopic and robotic prostate cancer surgery.

6. ACKNOWLEDGMENTS

This research was supported by an Idea Development Award from the Department of Defense Prostate Cancer Research Program, Grant #PC073709.

REFERENCES

[1] Burnett, A. L., Aus, G., Canby-Hagino, E. D., Cookson, M. S., D'Amico, A. V., Dmochowski, R. R., Eton, D. T., Forman, J. D., Goldenberg, S. L., Hernandez, J., Higano, C. S., Kraus, S., Liebert, M., Moul, J. W., Tangen, C., Thrasher, J. B., and Thompson, I., "Erectile function outcome reporting after clinically localized prostate cancer treatment," J. Urol. 178(2), 597-601 (2007).

[2] Wells, J., Kao, C., Jansen, E. D., Konrad, P., and Mahadevan-Jansen, A., "Application of infrared light for in vivo neural stimulation," J. Biomed. Opt. 10:064003, 1-11 (2005).

[3] Fried, N. M., Lagoda, G. A., Scott, N. J., Su, L. M., and Burnett, A. L., "Non-contact stimulation of the cavernous nerves in the rat prostate using a tunable-wavelength thulium fiber laser," J. Endourol. 22(3), 409-413 (2008).

[4] Wells, J. D., Thomsen, S., Whitaker, P., Jansen, E. D., Kao, C. C., Konrad, P. E., and Mahadevan-Jansen, A., "Optical mediated nerve stimulation: identification of injury thresholds," Lasers Surg. Med. 39, 513-526 (2007).

[5] Tozburun, S. and Fried, N. M., "Design of a compact laparoscopic probe for optical stimulation of the cavernous nerves," Proc. SPIE, vol. 716113, pp. 1-4, (2009).

[6] Tozburun, S., Mayeh, M., Lagoda, G. A., Farahi, F., Burnett, A. L., and Fried, N. M., "A compact laparoscopic probe for laser stimulation of the prostate nerves," IEEE J. Sel. Top. Quantum Electron. In Press.

Gaussian versus Flat-top Spatial Beam Profiles for Optical Stimulation of the Prostate Nerves

Serhat Tozburun[a], Gwen A. Lagoda[b], Arthur L. Burnett[b], and Nathaniel M. Fried[ab*]

[a] Department of Physics and Optical Science, University of North Carolina at Charlotte, NC
[b] Department of Urology, Johns Hopkins Medical Institutions, Baltimore, MD

ABSTRACT

The cavernous nerves (CN) course along the prostate surface and are responsible for erectile function. Improved identification and preservation of the CN's is critical to maintaining sexual potency after prostate cancer surgery. Noncontact optical nerve stimulation (ONS) of the CN's was recently demonstrated in a rat model, *in vivo*, as a potential alternative to electrical nerve stimulation (ENS) for identification of the CN's during prostate surgery. However, the therapeutic window for ONS is narrow, so optimal design of the fiber optic delivery system is critical for safe, reproducible stimulation. This study describes modeling, assembly, and testing of an ONS probe for delivering a small, collimated, flat-top laser beam for uniform CN stimulation. A direct comparison of the magnitude and response time of the intracavernosal pressure (ICP) for both Gaussian and flat-top spatial beam profiles was performed. Thulium fiber laser radiation (λ=1870 nm) was delivered through a 200-μm fiber, with distal fiber tip chemically etched to convert a Gaussian to flat-top beam profile. The laser beam was collimated to a 1-mm-diameter spot using an aspheric lens. Computer simulations of light propagation were used to optimize the probe design. The 10-Fr (3.4-mm-OD) laparoscopic probe provided a constant radiant exposure at the CN surface. The probe was tested in four rats, *in vivo*. ONS of the CN's was performed with a 1-mm-diameter spot, 5-ms pulse duration, and pulse rate of 20 Hz for a duration of 15-30 s. The flat-top laser beam profile consistently produced a faster and higher ICP response at a lower radiant exposure than the Gaussian beam profile due, in part, to easier alignment of the more uniform beam with nerve. The threshold for ONS was approximately 0.14 J/cm^2, corresponding to a temperature increase of 6-8 ^{o}C at the CN surface after a stimulation time of 15 s. With further development, ONS may be used as a diagnostic tool for identification of CN's during prostate cancer surgery.

Key Words: optical stimulation, nerve, prostate, cavernous nerves, neurovascular bundle

1. INTRODUCTION

The cavernous nerves (CN) are responsible for erectile function. Variation in size and anatomic location of the CN's among patients makes nerve preservation difficult during prostate cancer surgery. As a result, there is wide variability in sexual function rates (9-86%) following prostate surgery [1]. Any technology capable of improved identification and preservation of the CN's would result in improved sexual function and direct patient benefit.

Recently, optical nerve stimulation (ONS) has been demonstrated using pulsed infrared lasers [2]. ONS offers several advantages over electrical nerve stimulation (ENS), including: (1) a non-contact method of stimulation, (2) improved spatial selectivity, and (3) elimination of stimulation artifacts.

We have recently demonstrated successful ONS of the CN's in a rat model, *in vivo* [3]. This technique may have the potential to be used as an alternative method to ENS as a diagnostic tool for identifying and preserving the CN's during prostate surgery. However, a major limitation of ONS is that a narrow range of radiant exposures is necessary for safe, reproducible nerve stimulation. Radiant exposures less than ~ 0.35 J/cm^2 may not produce a reliable and a consistent ICP response, while higher radiant exposures of ~ 0.6-1.0 J/cm^2 may result in nerve damage with repetitive stimulation [3,4]. The laser beam diverges rapidly after exiting the fiber, making the beam diameter highly dependent on working distance. Therefore, it is critical that an ONS probe produce a collimated beam over a short working distance to provide a constant radiant exposure corresponding to safe, reproducible nerve stimulation.

*nmfried@uncc.edu; phone: 1 704 687 8149; fax: 1 704 687 8197

Preliminary work in our laboratory reported the design of an ONS probe with a collimated beam [5], and included fiber optic beam shaping methods for converting the Gaussian to flat-top beam profile with preliminary testing of the probe in a rat cavernous nerve model, *in vivo* [6].

The objective of this study is to directly compare the magnitude and response time of ICP as a function of radiant exposure for the Gaussian and flat-top spatial beam profile in a rat cavernous nerve model, *in vivo*. An ONS probe design capable of producing a fast and strong ICP response at a low radiant exposure would make the use of ONS more attractive as a diagnostic tool during laparoscopic and robotic nerve-sparing prostate cancer surgery.

2. MATERIALS AND METHODS

A 200-μm-core, low-OH silica optical fiber (BFL22-200, Thorlabs, Newton, NJ) with a 0.22 NA was used in these studies. The distal fiber tip was etched with hydrofluoric (HF) acid for 1 min at room temperature and then cleaned with distilled (DI) water. During the acid etching process, the fiber was surrounded by 49% HF acid diluted with DI water in a 1:4 ratio (acid/water). The central 100 μm of fiber tip was chemically etched to a depth of about 2 μm.

Computer simulations using fiber optic ray tracing software (RSoft Photonics CAD Suite Version 8.0.1.), based on advanced finite difference beam propagation techniques, were used to help optimize the chemical etching conditions necessary to provide a flat-top spatial beam profile.

A 5.5-Watt Thulium fiber laser (TLT-5, IPG Photonics, Oxford, MA) with a wavelength range of 1850-1880 nm was used for ONS. An aspheric lens (2-mm-OD, 350430-C, Thorlabs) and glass ferrule (Vitrocom, Mountain Lakes, NJ) were glued into place inside a quartz capillary tube (2.0-mm-ID, 2.4-mm-OD, CV2024, Vitrocom). Either an un-etched or etched 200-μm-core silica fiber (BFL22-200, Thorlabs) with 0.22 NA was inserted into a glass ferrule (Vitrocom) for centering with the optics, and then glued into place inside glass tubing. A green aiming beam and the infrared laser beam were coupled into the 200-μm fiber using a 12.7-mm-FL calcium fluoride lens. A thermal camera (A20M, Flir Systems, Boston, MA) was focused onto the nerve surface to record temperatures during ONS. Figure 1 shows a photograph of the rat surgical preparation and a diagram of the optical setup.

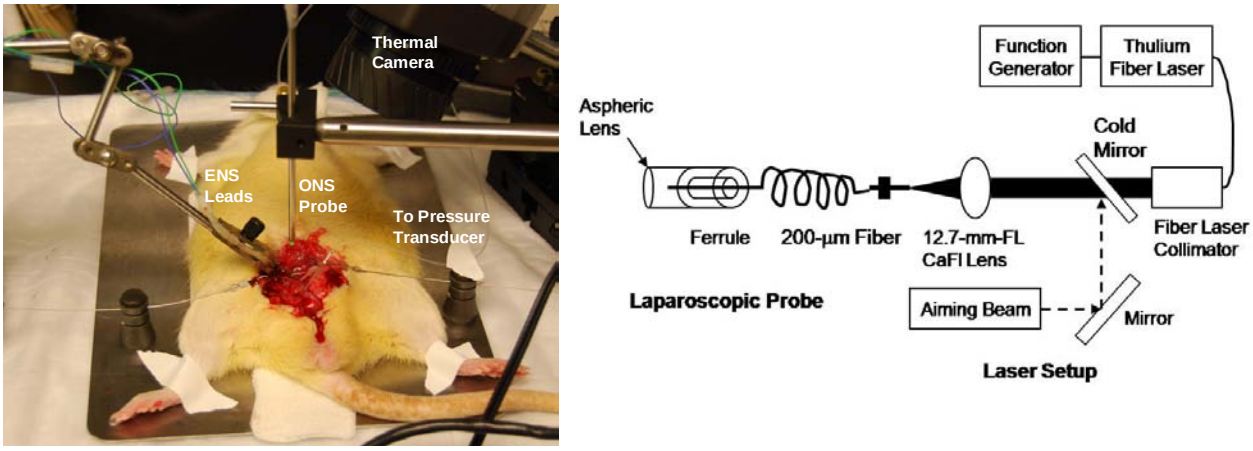

(a) (b)

Figure 1. (a) Photograph of surgical preparation for electrical and optical nerve stimulation. (b) Diagram of experimental setup.

3. RESULTS

Figure 2 shows the computer simulation results in both 2D and 3D formats. The laser beam propagates down the fiber with a Gaussian shape and then the beam is transformed to a flat-top profile in free space after traveling through the chemically-etched fiber tip. The aspheric collimating lens is placed at a distance of approximately 3.5 mm from the distal fiber tip, to capture and collimate this flat-top beam profile.

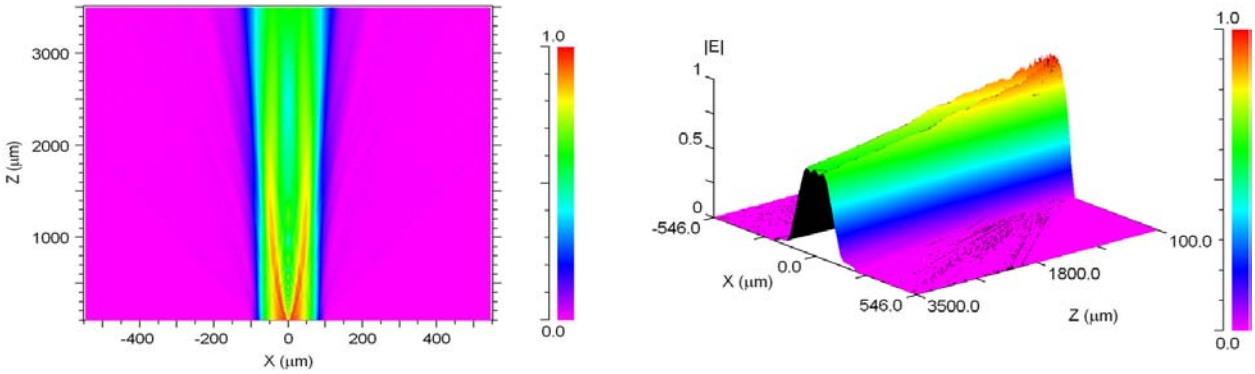

(a) (b)

Figure 2. Computer simulation shows transformation of laser spatial beam profile from Gaussian mode to flat-top mode in (a) 2D cross-section and (b) 3D after the beam propagates through the chemically-etched distal fiber tip.

The beam diameter was measured by performing razor blade scans at different distances from the output end of the probe. An approximately 1 mm ($1/e^2$) spot diameter and collimated beam was obtained over a working distance of 15-30 mm for both the (a) Gaussian (b) and flat-top probes (Figure 3).

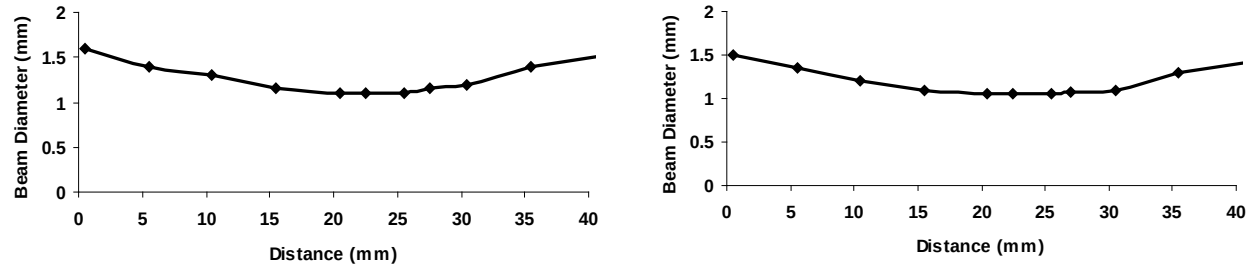

(a) (b)

Figure 3. Beam diameter of Gaussian (a) and Flat-top (b) probes as a function of working distance. The spot diameters remain at approximately 1 mm diameter over a working distance of 15-30 mm.

A direct comparison of the beam profiles for the un-etched and chemically etched fibers is shown in Figure 4. The un-etched fiber tip produces a Gaussian beam profile and the etched tip provides a relatively more uniform intensity distribution on the nerve surface as a flat-top spatial beam profile.

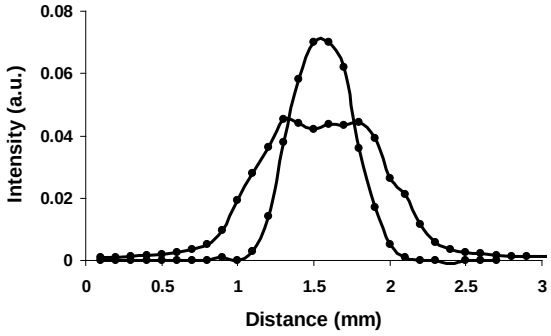

Figure 4. Comparison of spatial beam profiles at the distal fiber tip of un-etched and chemically etched fibers.

The spatial beam profiles at the output end of the (a,b) Gaussian and (c,d) flat-top probes are shown in Figure 5. The 2D and 3D images were acquired with an infrared beam analyzer (Pyrocam III, Spiricon, Logan UT).

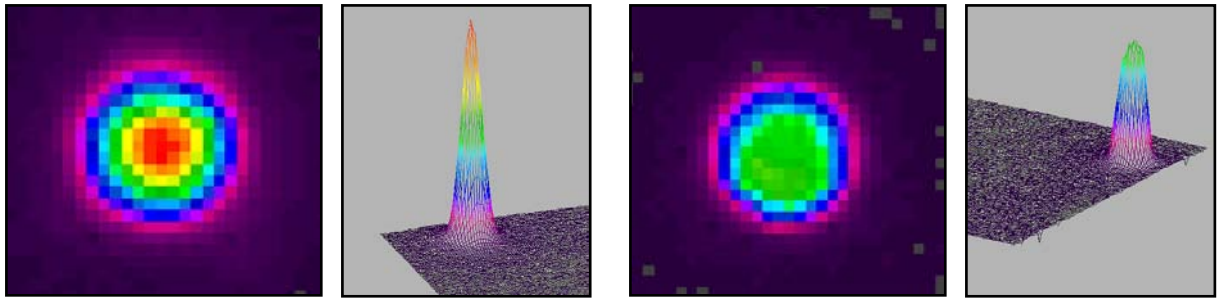

(a) (b) (c) (d)

Figure 5. Spatial beam profiles taken with an infrared beam analyzer: (a,b) Gaussian and (c,d) Flat-top spatial beam profiles.

Plots of the ICP response for the cavernous nerve for both Gaussian (a) and flat-top (b) spatial beam profiles as a function of radiant exposure are shown in Figure 6. The ONS parameters used in Figure 6a were 5-ms pulse duration, 20 Hz, and 1-mm-diameter laser spot, for a 30 s duration. In Figure 6b, the OSN parameters used were 5-ms pulse duration, 20 Hz, and about 1-mm-diameter laser spot, for a 15 s duration. The longer stimulation time in Figure 6a was necessary due to the weaker and slower ICP response time of the Gaussian beam profile. Faster and higher ICP responses of the CN were obtained at a lower radiant exposure for the flat-top versus the Gaussian beam profile. This may be due, in part, to improved alignment of a flat-top beam with the nerve by providing a more uniform intensity distribution across the nerve surface.

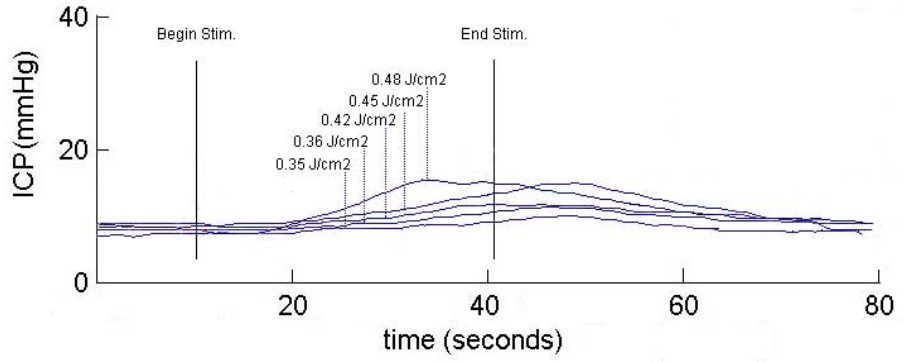

(a)

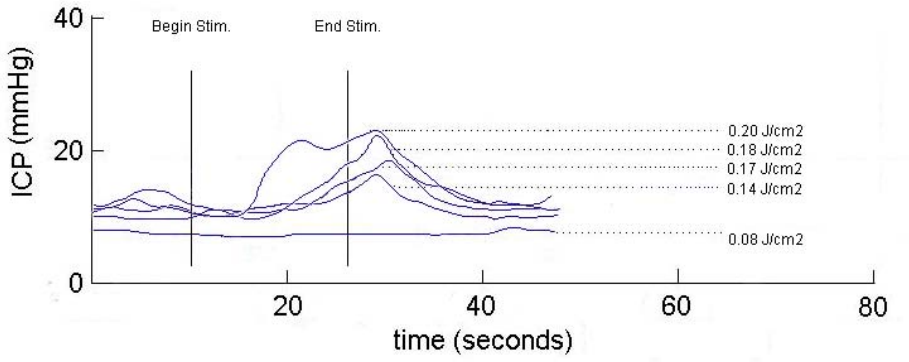

(b)

Figure 6. Comparison of (a) Gaussian and (b) flat-top spatial beam profiles for optical stimulation of the rat cavernous nerves as a function of radiant exposure. The magnitude of the ICP increases and the response time decreases as the radiant exposure is increased for both beam profiles. However, by comparison, the ICP response is significantly higher and faster for the flat-top beam profile at lower radiant exposures than for the Gaussian beam profile.

A thermal camera was used to record the temperature on the surface of the cavernous nerve during ONS (Figure 7). The minimum threshold for successful ONS, about 0.14 J/cm^2, as shown above in Figure 6b, corresponded to an increase in temperature of 6-8 ^{o}C (Figure 8a). This measurement is consistent with previous studies, which have shown that a temperature increase of 6-10 ^{o}C is necessary to produce ONS in peripheral nerves [7]. A temperature elevation of 6 ^{o}C was reached after approximately 6 s (Figure 8b) which also corresponds to the time delay between the beginning of stimulation and the ICP response observed in Figure 6b.

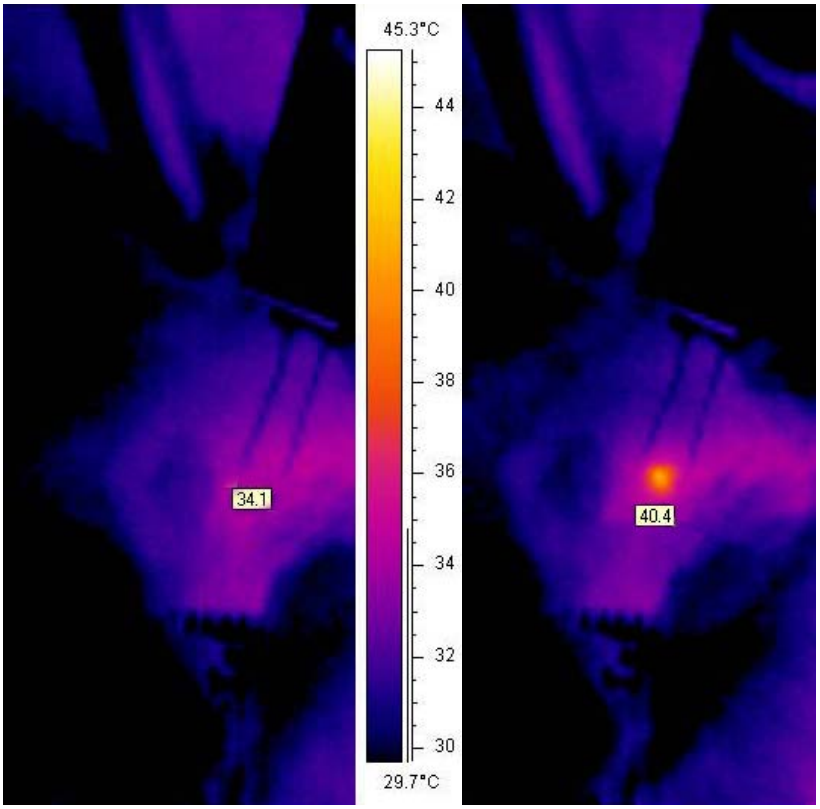

(a) (b)

Figure 7. Representative temperatures of the cavernous nerve surface during optical nerve stimulation with a radiant exposure of 0.14 J/cm^2 for 15 s: (a) Baseline nerve temperature just prior to stimulation; (b) Maximum temperature after stimulation.

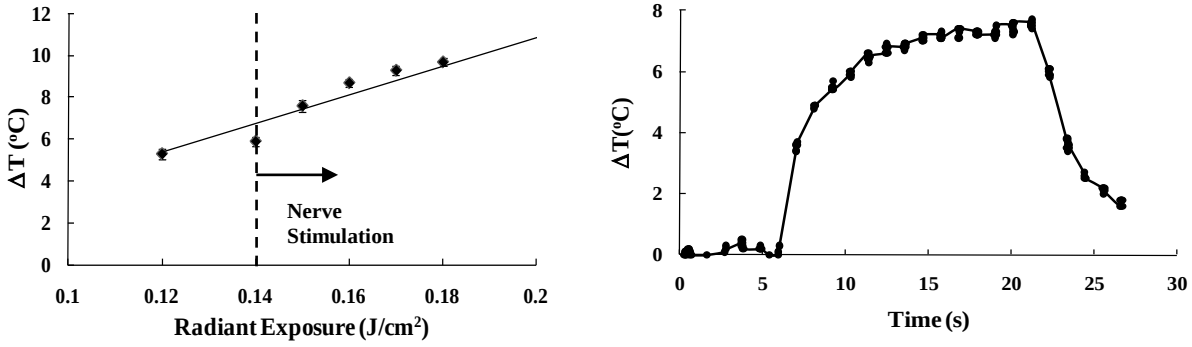

(a) (b)

Figure 8. The maximum change in temperature after optical stimulation (a) as a function of radiant exposure after 15 s stimulation, and (b) as a function of time for a fixed radiant exposure of 0.14 J/cm^2.

4. DISCUSSION

There is a wide variability in reported sexual potency rates following prostate cancer surgery, due, in part, to the difficulty in preserving the CN during surgery. Any technologies that can assist in identification and preservation of the CN during surgery may lead to direct patient benefit.

This study compares probes producing Gaussian and flat-top spatial beam profiles for ONS of the CN's in a rat model, *in vivo*. Both laparoscopic probes delivered a 1-mm-diameter, collimated beam at a working distance of about 20 mm from the CN. For the same laser parameters (pulse duration = 5 ms, pulse rate = 20 Hz), the flat-top beam profile produced a faster and higher ICP response at a lower radiant exposure than the Gaussian beam profile.

There are several limitations of this study that should be discussed. First, while the rat prostate is the standard small animal model for cavernous nerve studies, this model represents an idealized version of the prostate anatomy. Unlike the human prostate, the rat cavernous nerves are easily visible on the prostate surface. Further testing of our probe will be needed in a larger, canine prostate model which more closely resembles the human prostate.

Second, while the beam shaping method applied in this study resulted in a significant improvement in the uniformity of the spatial beam profile, a perfect "tophat" spatial beam profile was not achieved. Further reduction in the wings of the flat-top beam would provide even more uniform irradiation of the nerve surface during optical stimulation.

Finally, analysis of thermal damage to the nerve after laser nerve stimulation was based on nerve function in this study. Specifically, the ability to achieve a strong ICP response repeatedly with conventional electrical nerve stimulation immediately after laser stimulation was our primary source of feedback. In future studies, once the large matrix of laser nerve stimulation parameters and probe configurations have been fully optimized, histological analysis of the CN will need to be performed, as a more rigorous indicator of thermal damage. Chronic rat studies to determine whether there are any delayed thermal effects to the nerve will also need to be conducted.

5. CONCLUSIONS

A 3-mm-OD laparoscopic probe capable of delivering a collimated, 1-mm-diameter, flat-top laser beam was designed and successfully tested for optical nerve stimulation. This probe produced a faster and higher ICP response in the rat CN at a lower radiant exposure than for a standard probe with a Gaussian beam profile. With further development, this probe may be useful for safe and reproducible noncontact optical stimulation of the cavernous nerves during nerve-sparing laparoscopic and robotic prostate cancer surgery.

6. ACKNOWLEDGMENTS

This research was supported by the DOD Prostate Cancer Research Program, Grant #PC073709.

REFERENCES

[1] Burnett, A. L., Aus, G., Canby-Hagino, E. D., Cookson, M. S., D'Amico, A. V., Dmochowski, R. R., Eton, D. T., Forman, J. D., Goldenberg, S. L., Hernandez, J., Higano, C. S., Kraus, S., Liebert, M., Moul, J. W., Tangen, C., Thrasher, J. B., and Thompson, I., "Erectile function outcome reporting after clinically localized prostate cancer treatment," J. Urol. 178(2), 597-601 (2007).

[2] Wells, J., Kao, C., Jansen, E. D., Konrad, P., and Mahadevan-Jansen, A., "Application of infrared light for in vivo neural stimulation," J. Biomed. Opt. 10:064003, 1-11 (2005).

[3] Fried, N. M., Lagoda, G. A., Scott, N. J., Su, L. M., and Burnett, A. L., "Non-contact stimulation of the cavernous nerves in the rat prostate using a tunable-wavelength thulium fiber laser," J. Endourol. 22(3), 409-413 (2008).

[4] Wells, J. D., Thomsen, S., Whitaker, P., Jansen, E. D., Kao, C. C., Konrad, P. E., and Mahadevan-Jansen, A., "Optical mediated nerve stimulation: identification of injury thresholds," Lasers Surg. Med. 39, 513-526 (2007).

[5] Tozburun, S. and Fried, N. M., "Design of a compact laparoscopic probe for optical stimulation of the cavernous nerves," Proc. SPIE, vol. 716113, pp. 1-4, (2009).

[6] Tozburun, S., Mayeh, M., Lagoda, G. A., Farahi, F., Burnett, A. L., and Fried, N. M., "A compact laparoscopic probe for laser stimulation of the prostate nerves," IEEE J. Sel. Top. Quantum Electron. In Press.

[7] Wells, J., Kao, C., Konrad, P., Milner, T., Kim, J., Mahadevan-Jansen, A., and Jansen, E.D., "Biophysical mechanisms of transient optical stimulation of peripheral nerve," Biophys. J. 93(7), 2567-2580 (2007).

An Edge Detection Algorithm for Improving Optical Coherence Tomography Images of the Prostate Nerves

Shahab Chitchian and Nathaniel M. Fried
Department of Physics and Optical Science, University of North Carolina at Charlotte, 9201 University City Boulevard, Charlotte, NC 28223; Phone: 704-687-8149; Fax: 704-687-8197; Email: nmfried@uncc.edu

Abstract: The cavernous nerves, responsible for erectile function, are at risk of injury during prostate cancer surgery. An edge detection algorithm is presented here for improved OCT prostate imaging, and identification and preservation of the nerves.

OCIS codes: (170.7230) Urology; (110.4500) Optical coherence tomography; (100.2980) Image enhancement

1. Introduction

The cavernous nerves are responsible for sexual function. These nerves are at risk of injury during surgical dissection and removal of a cancerous prostate gland because of the close proximity of the nerves to the prostate surface. Their microscopic nature also makes it difficult to predict the true course and location of these nerves from one patient to another. These observations may explain in part the wide variability in reported potency rates (9-86%) following prostate cancer surgery [1]. Therefore, any technology capable of providing improved identification, imaging, and visualization of the cavernous nerves during prostate cancer surgery would aid preservation of the nerves and improve postoperative sexual potency.

Optical coherence tomography (OCT) is a noninvasive optical imaging technique for *in vivo* and *in situ* imaging of microstructure in biological tissues [2]. OCT imaging of the cavernous nerves in the rat and human prostate has recently been demonstrated [3-6]. However, improvement in the quality of the images for identification of the cavernous nerves is necessary before clinical use. Our laboratory has previously reported improvements in the image quality of OCT prostate images using denoising and segmentation techniques [7,8].

However, one of the main limitations in OCT remains the inability to image deep into opaque tissues. Currently, OCT is limited to an image depth of approximately 1 mm in prostate and periprostatic tissues. Therefore, in this paper, a new edge detection algorithm based on thresholding and spatial first-order differentiation is implemented to provide deeper imaging of the prostate gland.

2. Edge Detection System

A block diagram of the edge detection system is shown in Fig. 1. After luminance thresholding on the input image f(x,y), a first-order spatial differentiator of orthogonal gradient is performed to produce the differential image g(x,y) with accentuated spatial amplitude changes. Morphological post-processing is used to accentuate edges.

A. Luminance Thresholding: In this section, the glandular structure of the prostate is judged present if the luminance exceeds the threshold level of background.

B. Orthogonal Gradient Generation: After applying a threshold level to the denoised image f(x,y), a form of spatial first-order differentiation is performed in two orthogonal directions. In the discrete domain, the gradient in each direction is generated by [9]:

$$g_{r,c}(x,y) = f(x,y) * h_{r,c}(x,y) \tag{1}$$

where

$$h_r = \frac{1}{4}\begin{pmatrix} 1 & 0 & -1 \\ 2 & 0 & -2 \\ 1 & 0 & -1 \end{pmatrix}, h_c = \frac{1}{4}\begin{pmatrix} -1 & -2 & -1 \\ 0 & 0 & 0 \\ 1 & 2 & 1 \end{pmatrix} \tag{2}$$

are the row and column impulse response arrays for the 3×3 Sobel orthogonal gradient operator.

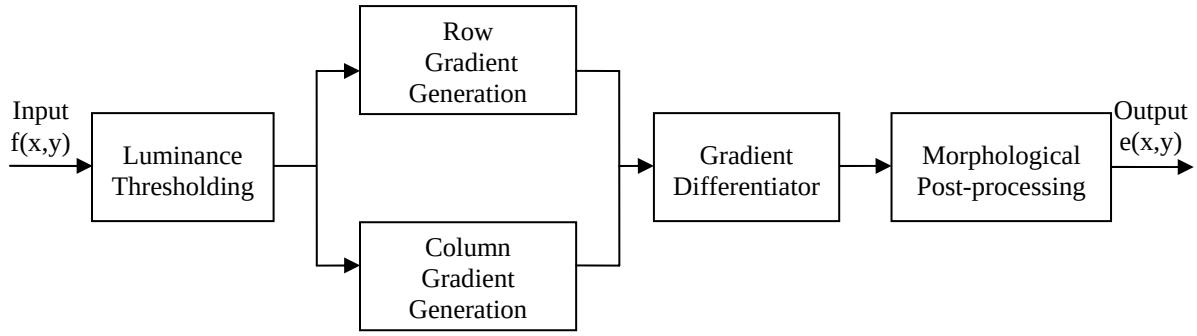

Fig. 1. Edge detection system block diagram.

The gradient amplitude is approximated by the magnitude combination

$$g(x,y) = |g_r(x,y)| + |g_c(x,y)| \qquad (3)$$

C. Morphological Post-processing: The morphological post-processing for accentuating edges proceeds by close operation. It is implemented by dilation followed by erosion.

3. Results

OCT images were taken *in vivo* using a clinical endoscopic OCT system (Imalux, Cleveland, OH) based on an all single-mode fiber (SMF) common-path interferometer-based scanning system (Optiphase, Van Nuys, CA). The OCT system was used with an 8 Fr (2.6-mm-OD) probe providing a lateral scanning distance of 2 mm and an image depth of 1.6 mm. The system was capable of acquiring real-time images with 11 μm axial and 25 μm lateral resolutions in tissue.

An unprocessed TD-OCT image of the cavernous nerve at longitudinal orientation along the surface of the rat prostate is shown in Fig. 2(a). Fig. 2(b) shows the combination of edge detection result of the denoised image and segmentation result. The edge detection approach was successful in accentuating prostate structures deeper in the tissue. The glandular structure of the prostate could be seen to a depth of approximately 1.6 mm in Fig. 2(b) in comparison with an only about 1 mm depth in the unprocessed OCT image in Fig. 2(a). However, it should be noted that further quantitative performance evaluation is difficult because of the lack of definitive performance criteria in the unprocessed OCT images. Overall, the edge detection technique enhanced structures deeper in the prostate gland.

It should be noted that the rat model used in this study represents an idealized version of the prostate anatomy because the cavernous nerve lies on the surface of the prostate, and is therefore directly visible. However, in the human anatomy, there may be an intervening layer of fascia between the OCT probe and the nerves, making identification more difficult. Since one major limitation of OCT is its superficial imaging depth in opaque tissues, an important advantage of the proposed algorithm is that the final processed OCT image should be able to provide deeper imaging in the tissue and using the segmentation approach we should be able to locate the cavernous nerve when it lies at various depths beneath periprostatic tissues.

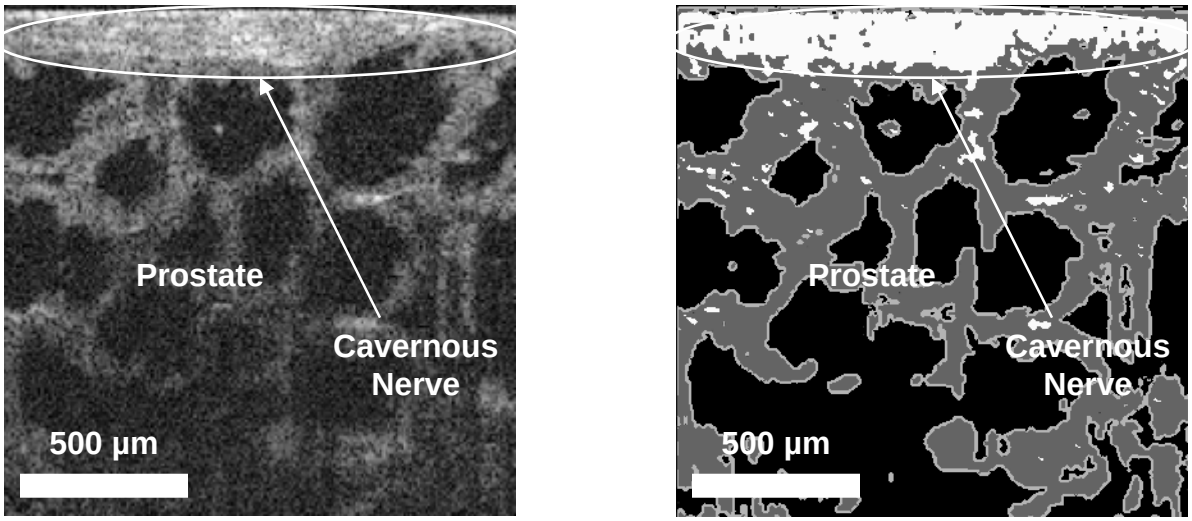

(a) (b)

Fig. 2. Longitudinal OCT images of the rat cavernous nerve: (a) Unprocessed; (b) Segmented and edge detected image.

4. Conclusions

In previous studies, a segmentation technique was used to locate the cavernous nerves in the prostate. An edge detection technique was applied here to complement segmentation to provide deeper imaging of the prostate gland. These algorithms for image enhancement of the prostate may be of direct benefit for implementation in clinical endoscopic OCT systems currently being studied for use in laparoscopic and robotic nerve-sparing prostate cancer surgery.

5. Acknowledgments

This research is supported by grants from the Department of Defense Prostate Cancer Research Program, Grant#PC073709, and the Department of Energy, Grant#DE-FG02-06CH11460. The authors thank Nancy Tresser of Imalux Corporation (Cleveland, OH) for providing the OCT system used in these studies.

6. References

[1] A. Burnett, G. Aus, E. Canby-Hagino, M. Cookson, A. D'Amico, R. Dmochowski, D. Eton, J. Forman, S. Goldenberg, J. Hernandez, C. Higano, S. Kraus, M. Liebert, J. Moul, C. Tangen, J. Thrasher, and I. Thompson, "Function outcome reporting after clinically localized prostate cancer treatment," J. Urol. **178**, 597-601 (2007).

[2] D. Huang, E. Swanson, C. Lin, J. Schuman, W. Stinson, W. Chang, M. Hee, T. Flotte, K. Gregory, C. Puliafito, and J. Fujimoto, "Optical coherence tomography," Science **254**, 1178-1181 (1991).

[3] M. Aron, J. Kaouk, N. Hegarty, J. Colombo, G. Haber, B. Chung, M. Zhou, and I. Gill, "Preliminary experience with the niris optical coherence tomography system during laparoscopic and robotic prostatectomy," J. Endourol. **21**, 814-818 (2007).

[4] N. Fried, S. Rais-Bahrami, G. Lagoda, A. Chuang, A. Burnett, and L. Su, "Imaging the cavernous nerves in rat prostate using optical coherence tomography," Lasers Surg. Med. **39**, 36-41 (2007).

[5] N. Fried, S. Rais-Bahrami, G. Lagoda, A. Chuang, L. Su, and A. Burnett, "Identification and imaging of the nerves responsible for erectile function in rat prostate, in vivo, using optical nerve stimulation and optical coherence tomography," IEEE J. Sel. Top. Quant. Electron. **13**, 1641-1645 (2007).

[6] S. Rais-Bahrami, A. Levinson, N. Fried, G. Lagoda, A. Hristov, A. Chuang, A. Burnett, and L. Su, "Optical coherence tomography of cavernous nerves: A step toward real-time intraoperative imaging during nerve-sparing radical prostatectomy," Urology **72**, 198-204 (2008).

[7] S. Chitchian, M. Fiddy, and N. Fried, "Denoising during optical coherence tomography of the prostate nerves via wavelet shrinkage using dual-tree complex wavelet transform," J. Biomed. Opt. **14**, 014031 (2009).

[8] S. Chitchian, T. Weldon, and N. Fried, "Segmentation of optical coherence tomography images for differentiation of the cavernous nerves from the prostate gland," J. Biomed. Opt. **14**, 044033 (2009).

[9] B W. Pratt, *Digital Image Processing* (Wiley, 2007).

ABSTRACT 9

2-D SEGMENTATION OF OCT PROSTATE IMAGES

Shahab Chitchian[1], Thomas P. Weldon[2], and Nathaniel M. Fried[1,3]

[1] *Department of Physics and Optical Science, University of North Carolina, Charlotte, NC*
[2] *Department of Electrical and Computer Engineering, University of North Carolina, Charlotte, NC*
[3]*Department of Urology, Johns Hopkins Medical Institutions, Baltimore, MD*

Introduction: The cavernous nerves, which are responsible for erectile function, course along the prostate surface and vary in size and location among patients, making identification and preservation of the nerves difficult during surgical removal of a cancerous prostate gland. Optical coherence tomography (OCT) has recently been tested for high-resolution *in vivo* imaging of the cavernous nerves in both rat and human prostates. However, improvements in the quality of OCT images are necessary before this new technology is suitable for clinical use. In this study, two-dimensional (2D) image segmentation is investigated to differentiate the nerves from the prostate gland.

Methods: 2-D rat prostate images acquired with a clinical endoscopic OCT system are segmented into three regions or classes: background, nerve, and prostate gland. To detect these classes, three image features were employed: Gabor filter, Daubechies wavelet, and Laws filter. The Gabor feature is applied with different standard deviations in the x and y directions. In the Daubechies wavelet feature, 8-tap Daubechies orthonormal wavelet is implemented, and the low pass sub-band is chosen as filtered image. Finally, Laws feature extraction is applied to the images. The features are segmented using a nearest-neighbor classifier. N-ary morphological post-processing is used to remove small voids.

Results: The cavernous nerves were differentiated from the prostate gland using this segmentation algorithm. The overall error rate measured only 0.058 and was obtained by manually creating a segmented image and comparing it to the automatic segmentation.

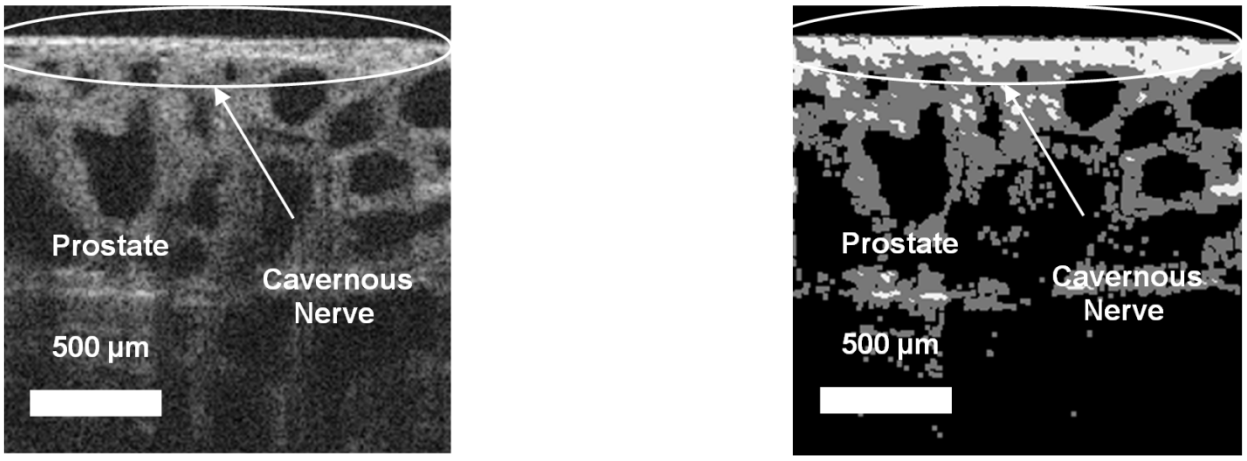

Figure 1. Representative OCT image of the rat cavernous nerve: (a) before; (b) after segmentation, showing the cavernous nerve in white, prostate tissue in gray, and background in black.

Conclusion: This algorithm for image segmentation of the prostate nerves may prove useful for implementation in clinical endoscopic OCT systems currently being explored for potential use in laparoscopic and robotic nerve-sparing prostate cancer surgery.

Acknowledgments: *This work was supported by an Idea Development Award from the Department of Defense Prostate Cancer Research Program, Grant #PC073709.*